View metadata, citation and similar papers at core.ac.uk

brought to you by CORE

provided by ASU Digital Repository

A Novel Mobile Device for Environmental Hydrocarbon Sensing and Its Applications

by

Yue Deng

A Dissertation Presented in Partial Fulfillment
of the Requirements for the Degree
Doctor of Philosophy

Approved April 2017 by the
Graduate Supervisory Committee:

Erica S. Forzani, Chair
Bin Mu
Heather Emady
Jeffery LaBelle
Mary Laura Lind

ARIZONA STATE UNIVERSITY
May 2017

ABSTRACT

The accurate and fast determination of organic air pollutants for many applications and studies is critical. Exposure to volatile organic compounds (VOCs) has become an important public health concern, which may induce a lot of health effects such as respiratory irritation, headaches and dizziness. In order to monitor the personal VOCs exposure level at point-of-care, a wearable real time monitor for VOCs detection is necessary. For it to be useful in real world application, it requires low cost, small size and weight, low power consumption, high sensitivity and selectivity.

To meet these requirements, a novel mobile device for personal VOCs exposure monitor has been developed. The key sensing element is a disposable molecularly imprinted polymer based quartz tuning fork resonator. The sensor and fabrication protocol are low cost, reproducible and stable. Characterization on the sensing material and device has been done. Comparisons with gold standards in the field such as GC-MS have been conducted. And the device's functionality and capability have been validated in field tests, proving that it's a great tool for VOCs monitoring under different scenarios.

DEDICATION

To my mom

ACKNOWLEDGMENTS

There are so many people to thank for helping me during the last five years. Ph.D study has never been fabulous but with so many people help and support, I have really enjoyed it and gained valuable experience.

First of all, I would like to express my greatest appreciation to my advisor Dr. Erica S. Forzani for the guidance and support of my Ph.D study and research with generous consideration and great patience. She is the most enthusiastic and optimistic person I ever met, no matter to research or life. Thank you so much for training me from a complete young student into a mature researcher with critical thinking ability. I cannot imagine a better mentor for my Ph.D study.

I would like to thank Dr. Jefferey LaBelle, Dr. Heather Emady, Dr. Mary Laura Lind, and Dr. Bin Mu for taking time to serve on my committee. It is grateful to have them as my committee members. They have provided a lot of valuable advises on my research from many other points of views.

I would like to thank Dr. Francis Tsow and Dr. Xiaojun Xian for their great guidance in my research. Their great help in polymer optimization, hardware design, and fabrication made my research went smoothly.

I would also like to thank Dr. Nongjian Tao, who provides invaluable advice and support on my research.

Last but not the least; I would like to thank my current and previous lab colleagues: Yueqi, Cheng, Ashley, Chenwen, Devon, Di, Dangdang, Anthony, Amelendu and Rui. It has been great pleasure working with you.

TABLE OF CONTENTS

Page

LIST OF TABLES ix

LIST OF FIGURES x

CHAPTER

1 BACKGROUND AND INTRODUCTION 1

1.Volatile Organic Compounds 1

2. Volatile Organic Compounds Detection – State of the Art 3

2.1 Gas Chromatography- Mass Spectrometry (GC-MS) 4

2.2 Photo Ionization Detection (PID) 5

2.3 Metal Oxide Semiconductor (MOS) 6

3. Quartz Tuning Fork (QTF) Resonator 8

4. Dissertation Overview and Summary 9

2 AGING EFFECT OF A MOLECULARLY IMPRINTED POLYMER ON A QUARTZ TUNING FORK SENSOR FOR DETECTION OF VOLATILE ORGANIC COMPOUNDS 10

1. Introduction 11

2. Material and Methods 12

2.1 Quartz Tuning Fork Sensors 12

2.2 Molecularly Imprinted Polymer (MIP) Coated QTF Sensors 13

2.3 Adsorption-Desorption Kinetics and Sensitivity Studies 14

2.4 Calibration Curve 15

CHAPTER Page

2.5 Apparatus 16

3. Results and Discussion 17

3.1 Sensitivity and Selectivity of MIP Modified Sensors 17

3.2 Aging Effect and Calibration Of QTF Sensors 19

3.3 MIP Aging Characterization 21

3.4 Binding Kinetic Analysis 25

3.5 Mitigation of Sensitivity Drop 31

4. Conclusion 32

3 ON THE STABILITY IMPROVEMENT AND ADSORPTION THERMODYNAMIC ANALYSIS -- A QUARTZ TUNING FORK BASED SENSOR FOR VOLATILE ORGANIC COMPOUNDS (VOCS) DETECTION 34

1. Introduction 35

2. Methods 36

2.1 Sensing Mechanism 36

2.2 Mitigation of Sensitivity Drop On Aged QTF Sensors 38

2.3 Temperature Effect Investigation 39

2.4 Thermal Stability Validation 39

2.5 Thermodynamic Analysis of the Adsorption Process 40

2.6 Van't Hoff Equation 41

3. Results and Discussion 42

3.1 Sensor Fabrication and Stability 42

CHAPTER Page

3.2 Temperature Effect 44

3.3 Thermodynamic Analysis 49

3.4 Thermal Stability Test Results 52

4. Conclusion 53

4 A NOVEL WEARABLE WIRELESS DEVICE FOR HYDROCARBONS DETECTION AND ITS FABRICATION 55

1. Introduction 56

2. Materials and Methods 59

2.1 Device Sensing Mechanism 59

2.2 Apparatus 59

3. Results and Discussion 62

3.1 Device Evaluation 62

3.2 Device Calibration, Selectivity of Sensors 65

3.3 Sensor QR Code 69

3.4 Personal VOCs Exposure Monitor 70

3.5 Device Comparison with Current Technology and Commercial Device 72

3.6 Device Validation under Different Scenarios 78

4. Conclusions 85

5 EXPLORATION ON RELATIONSHIP BETWEEN VOCS EXPOSURE WITH RESTING ENERGY EXPENDITURE 87

1. Introduction 88

CHAPTER Page

2. Materials and Methods 91

2.1 Capsaicinoids Extract Supplement, Capsimax®, Omnihealth Technology ... 93

2.2 Effect of Capsicum Extract Supplement on People's REE 93

2.3 Validation of REE Level and its Variance Correlation with Pops Exposure . 94

3. Results And Discussion 95

3.1 REE Measurement 95

3.2 Heart Rate Profile 98

3.3 Statistical Data Analyzation 99

3.4 Pre-Rated REE Change 101

3.5 REE Variance between Epidemiological Equations and Real Measurements 102

3.6 Relationship between ΔREE and Hydrocarbons Exposure 103

4. Conclusion 106

6 CONCLUSION AND FUTUREWORK 108

REFERENCES 110

LIST OF TABLES

Table Page

1.1 Example Vocs Exposure Limits from Different Standards 3

1.2 Comparison of Current Technologies in Vocs Detection..... 7

2.1 BET Surface Area Analysis Of MIP on Day 1 And Day 30 after Synthesis..... 23

2.2 Calculation of Binding Sites for MIP on the 1st and 30th Day after Synthesis .. 27

3.1 Energy Analysis on Adsorption..... 51

4.1 Device and Sensor Specifications..... 64

4.2 Parameters Used in QR Code 70

5.1 Summary of Participants..... 91

5.2 Information of Every Participant 92

5.3 Integrated Areas from Radar Plot 98

5.4 Paired T-Test between Capsaicinoids and Placebo Group 100

5.5 T-Test Between Female and Male Group..... 101

5.6 Pre-Rated REE Change..... 101

5.7 Summary of Hydrocarbons Exposure Level at Different Locations 106

LIST OF FIGURES

Figure Page

1.1 Sources of VOCs in 2005 1

1.2 Symptoms Associated with Exposure To Vocs 2

1.3 Schematic Diagram of a Gas Chromatograph 5

1.4 Schematic Diagramof Photo Ionization Detector 6

1.5 Schematic Diagram of Metal Oxide Semiconductor 7

2.1 A MIP Modified QTF Sensor 14

2.2 Response of TF Sensors Modified with Different MIPs. 18

2.3 MIP Selectivity. Response of MIP of Choice to Different Analytes 19

2.4 Sensitivity Drop on Sensors 20

2.5 SEM Images on Fresh and Aged MIP. 22

2.6 FTIR Spectra of MIP on The 1st and 30th Day after Synthesis 25

2.7 Adsorption Profile (Raw Data and Smoothed Fitting Curve) to 1ppm Xylene on The First Day and 30^{th} Day 26

2.8 Effect of Xylene Concentration on the Response Decrease after 30 Days. 29

2.9 Scheme 2.1. 30

2.10 Scheme 2.2.Hypothesis Scheme for the Aging Effect on Adsorption Cavity Sites of MIP.. 31

3.1 Schematic and Sensing Protocol of the VOC Monitor 38

3.2 Reproducibility of Sensor Fabrication Protocol on 200 QTF Sensors. A) Distribution of Coating Mass on QTF; B) Distribution of Reponse to 40ppm Xylene. ... 43

Figure Page

3.3 Stability Test on QTF Sensors. 44

3.4 Fresh QTF Sensor Calibration under Different Temperature. 46

3.5 Aged QTF Sensor Calibration under Different Temperature. 48

3.6 Van't Hoff Plot of: A) Fresh QTF Sensor; B) Aged QTF Sensor 50

3.7 Effect of Simulated 2-Day Shipping Condition on the MIP-Modified QTF Sensor. 52

4.1 Replaceable Sensor Cartridge and User Interface 62

4.2 Sensor Calibration Under Different Concentrations of O-Xylene. 66

4.3 Temperature Correction on Sensing Response 68

4.4 (A) Scanning Sensor QR Code; (B) Replacement of New Sensor Cartridge; (C) Real-Time Fitness and Vocs Exposure Device Data during Personal Exercise. 71

4.5 Comparison of the Response between the New VOC (TVOC) Device with a MIP-QTF Sensor and RAE Photo-Ionization Detector (PID) for Levels Assessed during a Trip on Los Angeles Highway 101. 73

4.6 Relative Response of VOC Device and Photo Ionization Detector for Levels Assessed during a Trip on Los Angeles Highway 101 74

4.7 Selectivity Validation Test to H_2S with Artificial Gas Sample 76

4.8 Outdoor Testing of Traffic Markers as a Function of Time 78

4.9 The New VOC Device's Performance to a Rapid Elevation Increase. Starting Point and End Point of the Trip Are Indicated Using Dashed-Dotted Lines. 79

4.10 Temperature Inversion Effect 81

Figure Page

4.11 Wind Speed and Direction Effect on VOC Device Performance 84

4.12 Real-Time Response of VOC Device to 40 Ppm Xylene on a Modified Tuning Fork Sensor. 85

5.1 Breezing® Device the Breezing® Indirect Calorimeter, Sensor Cartridge, Mouthpiece, and Iphone Interface of the Application. 90

5.2 A) Testing Protocol; B) Meal Provided to Participants 94

5.3 Average REE 96

5.4 ΔREE% at Different Time of the Test and Average. 97

5.5 Heart Rate Profile a) Zephyr Real-Time Activity Monitor; B) Average Heart Rate of All Participants 99

5.6 Difference between Mifflin-St Jeor Equation and Breezing REE. 103

5.7 Hydrocarbon Concentration at Different Locations Exposing to 17 Subjects .. 105

CHAPTER 1

BACKGROUND AND INTRODUCTION

1. Volatile Organic Compounds

Volatile organic compounds (VOCs), organic chemicals with high vapor pressure and low boiling point, are known as one of the major air pollutants for both indoor and outdoor environment [1, 2]. Exposure to VOCs has become an important public health concern. They are generated from biogenic sources and anthropogenic sources [3]. The main sources of indoor VOCs are paints, furniture, printers and so on. And for outdoor VOCs mostly come from vehicle emissions and industrial solvents [4]. Indoor VOCs level is usually 2-5 times higher than outdoor. Fig. 1.1 is an example from United States Environmental Protection Agency (EPA) [5] about VOCs sources.

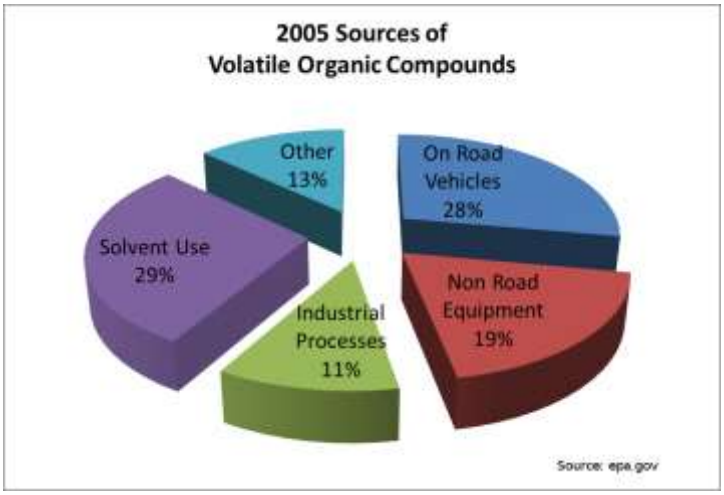

Figure 1.1 Sources of VOCs in 2005

According to the EPA, VOCs, specifically benzene, toluene, ethylbenzene and xylenes, are defined as class A pollutants due to their potential carcinogenic

characterization. This chemical group, also known as BTEX, may induce a lot of health effects such as respiratory irritation, headaches and dizziness [6-8]. Fig. 1.2 summarized the signs or symptoms associated with exposure to VOCs [5]. In our research, the main target analytes are hydrocarbons including aromatics and alkanes.

Figure 1.2 Symptoms associated with exposure to VOCs

Table 1.1 summarizes some examples of some chemical exposure limits from different organizations and standards. It includes major hydrocarbons that are potentially harmful to human health. These exposure limits and increasing concentration of air pollutants urge the need of developing new technology for easy real time monitor of user's living/working environment.

Table 1.1 Example VOCs exposure limits from different standards

Chemical	Exposure Limits
Benzene	NIOSH REL: TWA 0.1 ppm OSHA PEL: TWA 1 ppm
Toluene	NIOSH REL: TWA 100 ppm OSHA PEL: TWA 200 ppm 500 ppm (10-min max peak)
Octane	500 ppm
Hexachloroethane	1 ppm
Styrene	NIOSH REL*: TWA* 50 ppm (215 mg/m^3) OSHA PEL*: TWA 100 ppm C 200 ppm 600 ppm (5-min max peak in any 3 hrs)
Xylenes (o-, m-, p-)	NIOSH REL: TWA 100 ppm (435 mg/m^3) OSHA PEL: TWA 100 ppm (435 mg/m^3)

*TWA: Time weight average

REL: Recommend exposure limit

PEL: Permissible exposure limit

2. Volatile Organic Compounds Detection – State of The Art

To date, a number of different technologies have been developed for detection of VOCs in environment. The most popular ones include: gas chromatography (GC) in

combination with mass spectrometry (MS), photoionization detection (PID), metal oxide semiconductor (MOS).

2.1 Gas Chromatography- Mass Spectrometry (GC-MS)

Gas chromatography and mass spectrometry (GC-MS) are the most reliable technologies for quantification analysis of gases. In general, a gas chromatograph uses a column to separate different compounds based on their different retention time, which is the time used for each compound to pass through the column. As the compounds exit the end of the column, they are detected and identified electronically by the instrument (Fig. 1.3) [9, 10]. Mass spectrometer detects the compounds by ionizing the compounds to generate charged molecules or molecule fragments and measuring their mass-to-charge ratios. The compounds are firstly ionized by the instrument, and separated according to their mass-to-charge ratio. Those separated ions are then detected by a mechanism capable of detecting charged particles. The atoms or molecules can finally be identified by correlating known masses to the identified masses [10]. Although GC and MS techniques exhibit high accuracy in measurement of gas concentration, they are very expensive and bulky to be used for analysis of VOCs. In addition, other detection methods have been created and used to supplement MS, such as thermal conductivity (TCD) [11], differential mobility (DMD) [12], and flame ionization (FID) [13].

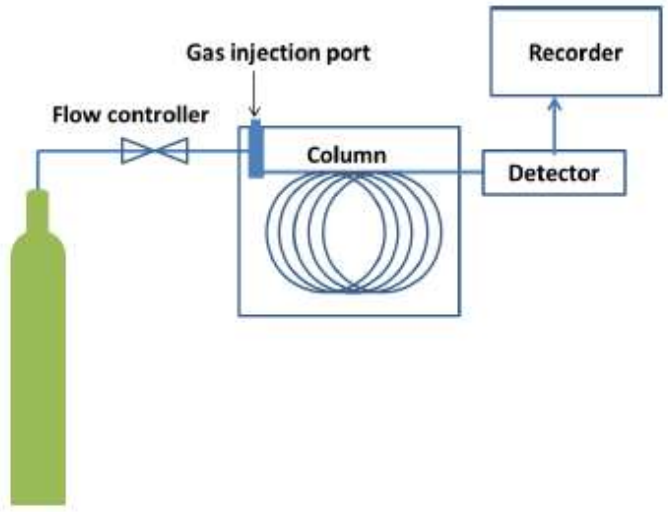

Figure 1.3 Schematic diagram of a gas chromatograph [9]

2.2 Photo Ionization Detection (PID)

PID has been particularly useful due to its portability. The gas sample is exposed to UV light (usually with an energy level of 10.6eV [14]), and VOCs are ionized due to the loss of electrons. The positively charged ions impact onto an electrometer, generating a current, which is then amplified and converted into a concentration value for display. There have been many patents regarding gas detection with PID [14, 15]. Due to the nature of detection, some non-VOC gases are also detected by PID [16, 17], and therefore the context of use is relevant for PID technology applications.

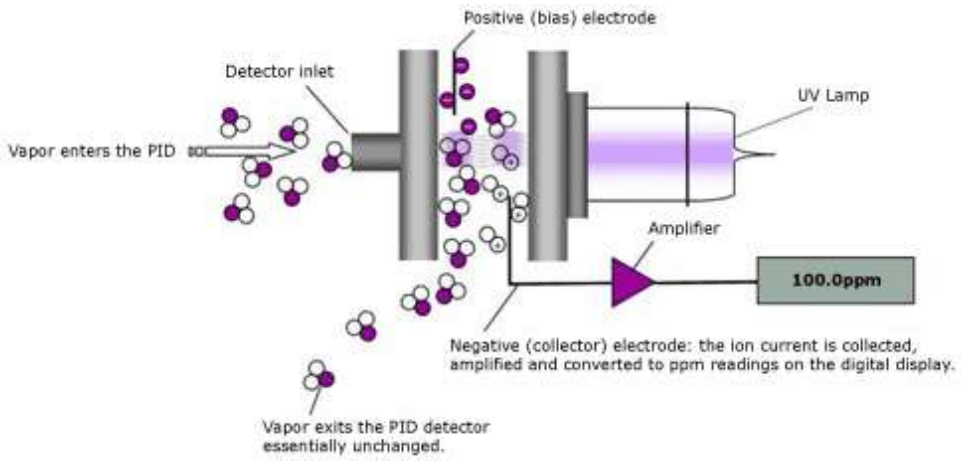

Figure 1.4 Schematic diagram of photo ionization detector [18]

2.3 Metal Oxide Semiconductor (MOS)

It has been known that with absorption and desorption of a gas on the surface of a MOS material, its conductivity will change [19]. By interacting (oxidizing or reducing) with the target gas, the charge carrier concentration of the MOS material will change [20, 21]. Research has demonstrated that MOS sensor responds to many kinds of VOCs such as methanol, ethanol, butanol and acetone [22]. However, selectivity and control of sensor response is a major challenge in this field [19]. And also, MOS sensor usually requires high operation temperature (300-400 ℃), which increases the power consumption significantly.

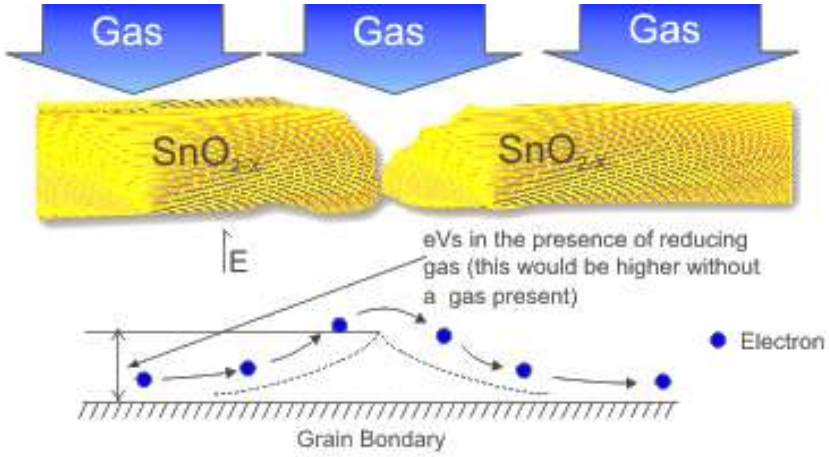

Figure 1.5Schematic diagram of metal oxide semiconductor [23]

The summary of above techniques is shown in Table 1.2.

Table 1.2 Comparison of current technologies in VOCs detection

Methodology	**Response sensitivity**	**Selectivity**	**Cost**	**Size**
Gas Chromatography-Mass Spectrometry	High sensitivity (down to part-per-trillion level)	High	High (>$10,000)	Big
Photo-ionization Detector	Good sensitivity (part-per-billion to part-per-million)	Low	Moderate (>$3,000)	Moderate
Metal Oxide Semiconductor	Good sensitivity (part-per-billion to part-per-million)	Low	Low (<$200)	Small

Thus, there is a need in the development of a small, low-cost, high sensitivity and selectivity, user friendly VOCs sensors that is capable for everyone to use anytime and

anywhere for a more complete and immediate assessment of people's exposure level to VOCs.

3. Quartz Tuning Fork (QTF) Resonator

Quartz tuning fork have been using in many applications which require precise timing, including wristwatch and microcontroller integrated circuit. Quartz is a piezoelectric material, which means application of mechanical stress results in generation of an electrical signal and vice-versa, and that's the basic principle used in the operation of the quartz tuning fork. Mechanical resonations are generated when a voltage is applied the prongs. The tuning forks require very low power consumption and are very stable and precise [24-26].

Resonant frequency of a tuning fork can be expressed as follows:

$$f_0 = \frac{1}{2\pi}\sqrt{\frac{k}{M}} \qquad 1\text{-}1$$

Where k represents effective spring constant and m is mass of the tuning fork. In chemical sensing, people usually modify the QTF surface with a selective sensing material. The material forms a thin layer on the prongs, and binds with the target analyte. Once the analyte is bound with the polymer on the prongs, the mass of the prongs increase and therefore decrease the resonant frequency. The change of the frequency is given by:

$$\Delta f(k, M) = \left(\frac{f_0}{2}\right)\left[\frac{\delta k}{k} - \frac{\delta M}{M}\right] \qquad 1\text{-}2$$

And based on the mass change, the concentration of the target analyte can be calculated. These commercially available (US $0.01/each) tuning forks are a great for portable chemical sensors.

4. Dissertation Overview and Summary

This document consists of 6 chapters. Chapter 1 (this chapter) provides an overview of background in VOCs detection and state of art techniques. Chapter 2 discusses the selective material, molecularly imprinted polymer (MIP), for VOCs detection (based on QTF) and its characterization. In chapter 3, the stability and thermal effect of the MIP modified QTF sensor is mainly studied. And chapter 4 presents the integration of a wireless and wearable VOCs monitor for personal use and its validation in field.

Resting energy expenditure, also known as metabolism, is a critical factor that helps in weight management. It has been reported that exposure to certain kind of VOCs may potentially influence on weight loss [27]. Chapter 5 presents research that assesses the relationship between individual VOCs exposure level and metabolism.

In summary, a handheld wearable device for VOCs exposure monitor is implemented and validated. It can be applied to both indoor and outdoor VOCs monitoring for daily air quality assessment.

CHAPTER 2

Aging effect of a Molecularly Imprinted Polymer on a Quartz Tuning Fork Sensor for Detection of Volatile Organic Compounds

ABSTRACT

The sensing selectivity, stability and sensitivity of a molecularly imprinted polymer (MIP) selective to the adsorption of hydrocarbons was studied. The MIP was deposited on a quartz crystal tuning fork (QTF) resonator, whose chemical and physical properties were monitored over time, using Scanning Electron Microscopy (SEM), Brunauer–Emmett–Teller adsorption isotherm analysis (BET), and Fourier transform infrared spectroscopy (FTIR). In addition, kinetic binding analysis of the MIP-modified QTF sensor was carried out for the sensors stored and operated under ambient conditions (740 mmHg, 20-23^{o}C). Although the polymer was able to maintain its physical and chemical properties at microscopic, BET adsorption, and spectroscopic levels, the intrinsic adsorption properties of hydrocarbons onto MIP binding sites altered over time, which suggest that the 3-D conformational changes of the polymer binding sites occurring at nanoscopic/angstrom level may cause the sensitivity degradation in MIP. The changes were significantly reduced by mixing the polymer with “organic glue”, polystyrene and store under low temperatures.

1. Introduction

Volatile organic compounds (VOC) are organic chemicals emitted from anthropogenic and biogenic sources with significant vapor pressure [1, 2]. According to the United States Environmental Protection Agency (EPA), VOCs are one of the major pollutants for indoor and outdoor air quality since they are emitted from furniture, appliances, and construction materials as well as incomplete combustion of fuels (cars, trucks). Most of VOCs are harmful to health, especially the respiratory system [28], and therefore, there is a need of determining personal exposure concentrations. Along this line, a plethora of analytical methods have been developed to monitor VOC concentrations. Among them, the most popular ones are photo-ionization detection (PID) and gas chromatography-mass spectrometry (GC-MS). In addition, other detection methods have been created and used to supplement GC, such as thermal conductivity (TCD) [29], differential mobility (DMD) [30], and flame ionization (FID) [13].

As mentioned in chapter 1, for the need of personal exposure monitoring, some personal VOC monitors have been recently developed [13]. One example is a wearable wireless monitor developed by our group. The monitor is based on quartz crystal tuning forks (QTF) sensors for environmental VOCs [31-33]. Similar to QCM resonator, quartz tuning forks are mass sensitive resonators useful in biosensors [24, 26]. In the wearable wireless monitor, the QTF sensors are coated with polymer films that are sensitive and selective to target VOCs. For instance, molecularly imprinted polymers (MIP) are highly selective to hydrocarbons, which are carcinogens or potential carcinogens. The molecularly imprinted polymers are formed in the presence of a specific molecule

template that is extracted afterwards, leaving binding site complementary cavities with chemical affinity to the molecules similar to the original molecule template or its family [34].

Many studies have been done on the molecularly imprinted polymer structure [34], including thermal stability [35], and chemical and physical adsorption calculations and evaluations [36-38]. However, there are no former systematic studies of MIP aging. For the first time, this work demonstrates evidences of MIP aging and its effect on MIP sensing properties. We have built MIP-modified QTF sensors, and systematically tested the stability of the material. MIP is a porous and adsorptive sensing material [39-41], and we have observed an interesting aging effect on the sensing material with a concomitant decay of sensor sensitivity over time. To better understand the adsorption/desorption kinetics and physical/chemical transformation of the MIP, we have investigated the structural changes in the polymer, as well as the number of selective binding sites using several techniques. We have also studied the stability of MIP-modified QTF sensors under real operative conditions, and proposed a mechanism behind the sensitivity degradation. With the ultimate goal of achieving sensitive and stable sensor with long shelf-time, we have explored a solution to minimize the sensitivity degradation in MIP.

2. Material and Methods

2.1 Quartz Tuning Fork Sensors

The QTFs are piezoelectric crystal resonators with high mass sensitivity, thermal and mechanical stability, and self-sensing capability [42]. The QTF sensors used in the

present experiments have a native resonant frequency of 32.768 KHz and a dimension of 4 mm x 0.6 mm x 0.35 mm (manufactured by Jiangcheng Electronic Limited Company), which renders a mass sensitivity of 20 ng/mm^2.

2.2 Molecularly Imprinted Polymer (MIP) Coated QTF Sensors

2.2.1 Polymer Preparation

The MIP is synthesized using divinylbenzene (mixture of o-, m-, p-, Sigma Aldrich) as both monomer and cross-linker, o-xylene (Sigma Aldrich) as both template and solvent, and azobisisobutyronitrile (AIBN, Sigma Aldrich) as initiator, under argon environment, 85 ℃, and overnight. In addition, MIPs using styrene (Sigma Aldrich) and the above mentioned components were synthesized to study the effect of the ratio of monomer (styrene)-to-cross-linker (divinylbenzene) on the sensitivity of the polymer to xylene.

2.2.2 Polymer Treatment and QTF Sensor Coating

After synthesis, the polymer is broken into smaller pieces (estimated size: 1mm-5mm) first and smashed using ball milling machine (PQ-NO 4 Planetary Ball Mill, Across International) to obtain consistent particle size. The uniform polymer particles (estimated size: 1 μm-10 μm) are then dispersed in o-xylene solvent and the mixture is casted onto QTFs with a metal needle syringe. An optical image of a modified QTF sensor is shown in Fig. 2.1. The commercial quartz tuning fork are built in a way that the fragile prongs are protected in a metal can; this can also protect the prongs from outside pressure variation and other potential disturbances. In order to use tuning fork as

chemical sensor, it need to be modified. We removed the metal can enclosing the prongs, exposing the prongs of the tuning fork.

Figure 2.1 A MIP modified QTF sensor

2.3 Adsorption-Desorption Kinetics and Sensitivity Studies

In order to study the adsorption-desorption kinetics and sensitivity, we used a wireless personal monitor, which consists of four functions: **a)** Collection and Delivery: the air sample is collected and delivered via an alternating valve-activated mechanism with a purging channel and a sampling channel. In the purging channel, particulates and VOCs from air are filtered out with a zeroing filter for 120 seconds, producing a particulate and VOC-free air sample that is used for baseline assessment of the MIP-modified QTF sensors. In the sampling channel, particles in the sampled air are filtered out, producing a 60 seconds sample for testing hydrocarbons. Before entering the sensing chamber, sample gas will pass through a Nafion® tube for humidity balancing. **b)** Sensing and Detection: after the air sample is produced, it passes a sensor chamber with a MIP-modified QTF sensor, and an unmodified QTF that serves as a reference sensor. The two QTF sensors are placed in-line along the flow direction for detection, and the differential sensing signal between the MIP-modified QTF and unmodified QTF sensor is

assessed. **c)** Converting chemical binding events to a readable electronic output: the resonant frequency shifts of QTF sensors upon changes in its mass, which thus allows us to detect the mass change due to the adsorption of molecules in MIP by measuring the frequency shift. **d)** Data transmission and signal processing: the differential sensor signal is transmitted to a recording system via Bluetooth®, where the signal is captured as raw signal, and further processed as concentration output. The recording system is a custom-designed application used on a smart phone, which helps and supports users to assess instantaneous concentration readings.

In this chapter, we define sensor response as the resonant frequency shift on QTF sensors after the 1 min period of sampling.

2.4 Calibration Curve

Using the above-described setup, we obtained the calibration curves with differential sensor signal of frequency (Δf/Hz) under different concentrations of gas samples, including 0 ppm (clean air), 1ppm, 20ppm, 40ppm, 80ppm, and 160ppm. O-xylene was chosen as the model analyte. Air samples were prepared in laminated bags with clean and dry air balance. All air samples' concentration was also monitored using PID as a reference. Tests were processed under ambient conditions on the first day and 30 days after the sensor was prepared. During storage period, the sensors were kept under ambient condition undisturbed. In addition, the response of the MIP-modified sensor stored at ambient conditions was monitored for consecutive days at normal pressure and temperature conditions (740 mmHg and 20-23 ^{o}C).

2.5 Apparatus

2.5.1 SEM

Scanning Electron Microscope (SEM) Philips XL30 SEM was used to study the surface morphology of MIP-modified QTF sensors at an applied voltage of 15kV.

2.5.2 Brunauer–Emmett–Teller (BET) Method

BET method was used to measure specific surface area and perform porosity analysis, including mesopore size and volume. A Tristar II 3020 BET instrument from Micromeritics was used on freshly prepared MIP samples and heat pretreated MIP samples exposed to nitrogen for 11 hours at 50℃.

2.5.3 Fourier Transform Infrared Spectroscopy (FTIR)

A Nicolet 6700 FTIR spectrometer from Thermo Electron Corporation was used to obtain FTIR spectra of fresh and aged MIP samples.

2.5.4 Mitigation of Sensitivity Drop

To ensure the stability of the QTF sensors, the polymer was mixed with O-xylene dissolved polystyrene solution with a mass ratio of 19:16. Storage of MIP-modified sensors at 4 ^{o}C was used to mitigate sensitivity drop (see results and discussion). Other fabrication process was same as above.

3. Results and Discussion

3.1 Sensitivity and Selectivity of MIP Modified Sensors

Fig. 2.2 shows the sensor performance for different MIP synthesis recipes, including different monomer (styrene) to cross-linker (DVB) ratios. Comparing to pure polystyrene, MIPs synthesized with template molecule will have a response 26 to 35 times higher than the corresponding response to polystyrene. In addition, the lower ratio of monomer to template, the higher the performance response, and therefore, the MIP synthesized with no monomer, and 100% cross-linker (molar ratio of 0:1:2 in monomer, template and crosslinker.) was the option of choice for this work. We hypothesize that the higher the crosslinking degree, the higher the number of micro/nano cavities inside the polymer that leads to a higher response.

Many works have been reported about sensing VOCs using MIP modified piezoelectric sensors [43]. They have shown effective ways of MIP synthesis [44, 45]. Related literature shows a sensing response range of 0-4.99 mg/g to p-xylene [44], while our MIP response range is 0-4.09 mg/g to o-xylene. This fact indicates comparable performance of our MIP to previous reported work.

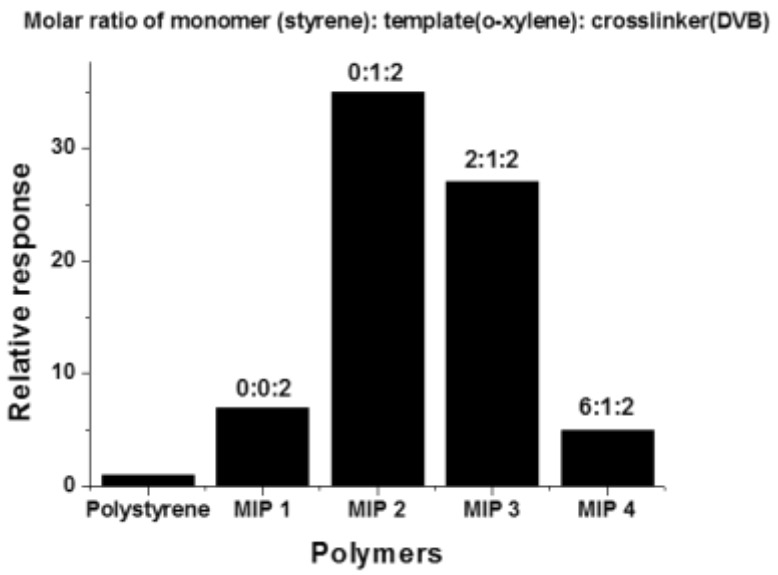

Figure 2.2 Response of TF sensors modified with different MIPs. The MIP-modified TF sensor response is normalized to the PS-modified TF response. Different MIPs were synthesized with different ratios of styrene as monomer, o-xylene as template, and divinylbenzene (DVB) as cross linker. The MIP synthesized with no monomer (styrene), and pure cross-linker (DVB) had the higher sensitivity, and was selected as MIP of choice.

Due to the synthesis mechanism, molecularly imprinted polymer has specific selectivity to the template molecule. To assess the effectiveness of polymer synthesis, we tested the MIP modified QTF sensors' response to different gas analytes. As shown in Fig. 2.3, the response of QTF sensor is different within different analytes. Fig. 3 shows the polymer has a good selectivity to VOCs family, especially aromatics, and hydrocarbons compounds, contributing to binding with π-π stacking and van der Waals forces interactions. Previous literature work [46] has shown high selectivity of MIP

towards analytes used as template, and solvent in the polymer synthesis. The solvent act as template, and leaves behind a specific cavity once evaporates from the synthesized structure. The method of synthesis offers a convenient way to produce polymers with significantly high selectively to target "solvent" molecules.

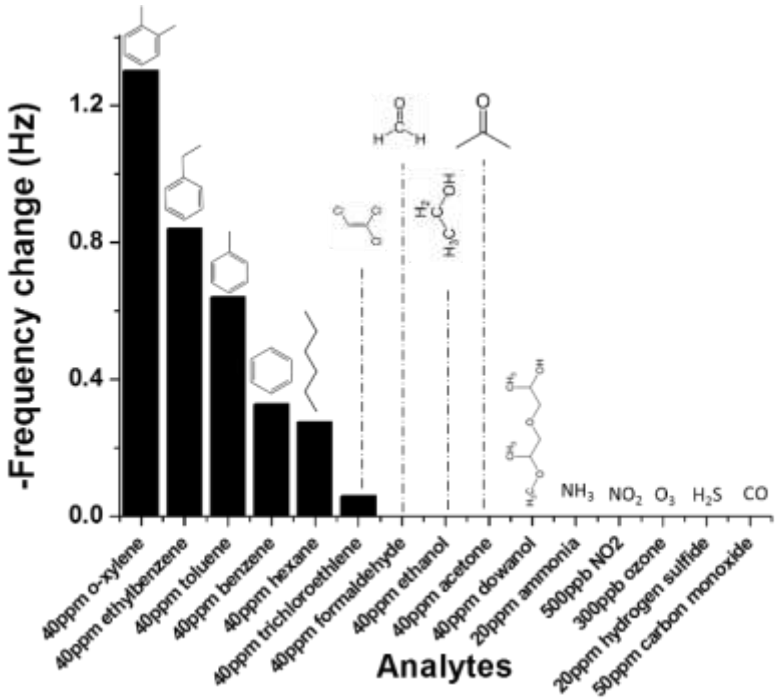

Figure 2.3 MIP selectivity. Response of MIP of choice to different analytes

3.2 Aging Effect and Calibration of QTF Sensors

Four MIP-modified QTF sensors were prepared to evaluate the sensor response as a function of storage time at ambient conditions as described in the experimental section. A o-xylene concentration of 1 part-per-million volume in volume (ppmV) was used for testing the steady-state response on the 1st, 7th, 11th, and 15th day after preparation (Day 0) (Fig. 2.4A). As shown in Fig. 4A, the responses of all the sensors decayed to 3%-5% of

the initial response after 30 days. In addition, calibration curves of the sensors on Day 1 and Day 30 (Fig. 2.4B) showed overall sensitivity decay across 1 to 160 ppm o-xylene concentration range. Langmuir adsorption isotherms were used to fit the response-concentration behavior of the sensors. Fitting squared-regression coefficients (r^2) were close to 1, indicating relatively good agreement with a monolayer gas adsorption model. Therefore, a gas absorption process expressed as: $A + B \rightleftharpoons C$, where A is the analyte gas molecule, B is the effective binding site of the polymer, and C is the occupied (unavailable) binding site was assumed.

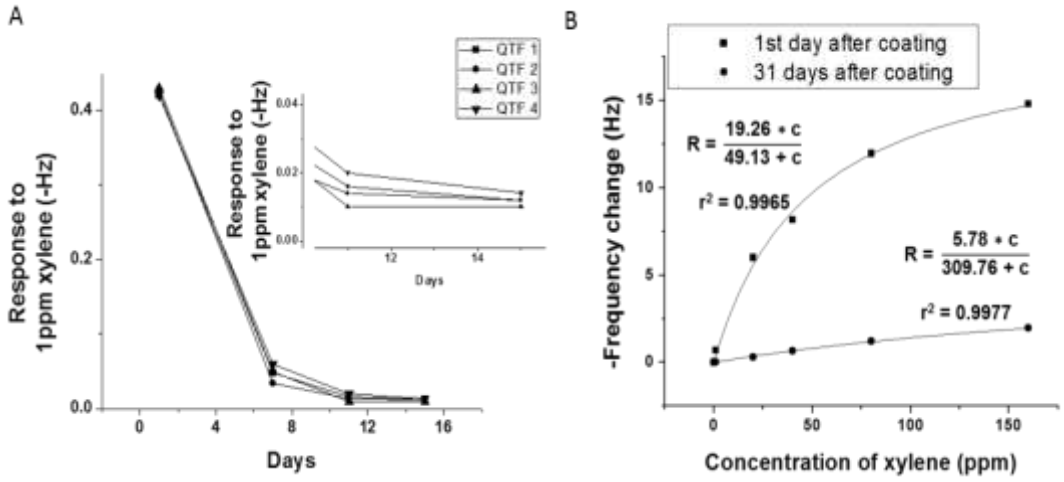

Figure 2.4 Sensitivity drop on sensors (A) MIP-modified QTF sensor response to 1 ppmV xylene vs. time for four sensors (day 1 corresponds to the day of MIP-modified QTF sensor preparation). The inset is a zoom in of the response from 10 to 14 days. (B) Calibration curves of the MIP-modified sensor (frequency change vs. xylene concentration) on Day 1 and Day 30 after preparation (see text for details of equations and fitting).

Langmuir Equation can be written as [47]:

$$R = \frac{R_{max} * c}{K_D + c} \qquad 2\text{-}1$$

where R is the mass of adsorbed gas, which is proportional to the differential frequency change of QTF sensors, R_{max} is maximum amount of adsorbed gas that is represented by the maximum differential frequency change from the QTF sensors, and proportional to the maximum amount of analyte binding sites, c is the o-xylene gas concentration, and K_D is dissociation constant, which is defined as:

$$K_D = \frac{[A][B]}{[C]}. \qquad 2\text{-}2$$

where [A], [B] and [C] are concentration of species [A], [B] and [C] respectively. The well-fitted calibration curve indicates that R_{max} drops 70%, from 19.26Hz to 5.78Hz, while K_D increases 530%, from 49.13 ppm to 309.76 ppm. The changes were indicative of significant changes in both number strongly suggest conformation and/or chemical nature of the binding sites, and therefore, they were further investigated (see below).

3.3 MIP Aging Characterization

3.3.1 SEM Analysis

We took SEM images of the MIP on the Day 1 and Day 30 after synthesis. Fig. 2.5 A) and B) show the MIP polymer particles deposited onto the QTF sensor before and after aging of 30 days at normal ambient conditions. It is worth noticing the particle size and morphologic features of the fresh (Day 1) vs. aged (Day 30) MIP polymer do not show significant changes in terms of surface morphology and particle size, indicating that there is no significant change of the polymer morphology at microscopic level.

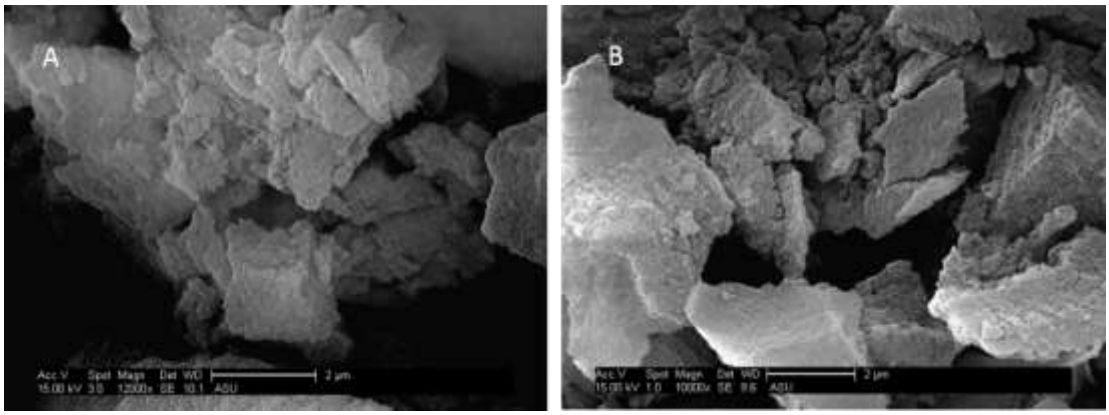

Figure 2.5 SEM images on fresh and aged MIP (A) SEM image of a freshly prepared MIP (B) SEM image of MIP kept in normal ambient condition for 30 days.

3.3.2 BET Analysis

To further quantify the gas adsorption capabilities of the polymer, MIP samples with fresh (Day 1), and aged (Day 30) polymer were analyzed, using Brunauer–Emmett–Teller (BET) surface area analysis. Table 2.1 summarizes the results, where the BET surface area, pore size, and BHJ pore volume remained unchanged over the 30 days period. However, since BET analysis is based on sample's physical adsorption of nitrogen, and N_2 is much smaller than o-xylene in terms of molecular size, the results thus imply that our MIP polymer has a physically stable porous structure towards the adsorption of N_2.

From SEM images and BET analysis, it was concluded that the sensitivity decay effect is not caused by physical structural changes. Therefore, two hypotheses on the reduction of MIP sensitivity arose.

Hypothesis *I*- The change in MIP sensitivity may be originated from a change in chemical moieties, and therefore, a change in chemical adsorption.

Hypothesis II- Chemical moieties remain unaltered, and the change in MIP sensitivity may be originated by a morphology change at sub nanometer/Angstrom level.

Table 2.1 BET surface area analysis of MIP on Day 1 and Day 30 after synthesis.

	1st day	**30th day**
BET surface area/m^2 g^{-1}	599.6	598.7
Pore size/nm	5.2	5.2
BJH* pore volume/cm^3 g^{-1} (pores between 1.7nm and 300.0nm width)	0.7	0.7

BJH: Barrett-Joyner-Halenda (BJH) analysis, a pore size distribution determination method, which is typically applied to nitrogen desorption data.

3.3.3 FTIR Analysis

In order to explore potential chemical functional changes in MIP polymer, FTIR spectrums were obtained on MIP fresh polymer (Day 1), and on MIP aged polymer (Day 30 and beyond). The spectra in Fig. 2.6 shows dibasic structural bend vibration of phenyl group at 795.8 cm^{-1} and 704.0 cm^{-1}, phenyl group skeletal vibrations at 1438.5 cm^{-1}, 1492.3 cm^{-1}, 1526.7 cm^{-1}, and 1606.3 cm^{-1}, water vibrations at 2049.7 cm^{-1} to 2323.1 cm^{-1}; carbon–hydrogen bond of aromatic rings stretching vibrations at ~2917 cm^{-1}; double bonds of functional monomers (unreacted DVB) at 995.3 cm^{-1}. The chemical functional groups of polymer on Day 1 and Day 30 are identical, in terms of quality and quantity, thus implying the polymer maintained its chemical moieties. In addition, we have not observed the presence of ketones, aldehyde, or carboxylic groups, which are typically

reaction products of double bonds with potential oxidizing agents such as NO_x or O_3, typically present in ambient air [48].

In summary, fresh and aged polymers were characterized via SEM, BET adsorption, and FTIR, and no obvious change in either physical surface morphology or chemical properties was found. Therefore, the significant sensitivity change on MIP-modified QTF sensors was attributed to 3-D structural changes at length scales that are not evidenced by SEM and BET (*Hypothesis II*). In fact, o-xylene molecule used as analyte has a molecule size of ~7Å [49]; while nitrogen is significantly smaller at ~3Å [50]. Therefore, N_2 adsorption is not affected since it is a small molecule. On the contrary, the adsorption of the bigger xylene is affected, and therefore, possibly changes taking place at the 3-7 Angstrom level may cause changes of xylene adsorption (see representative schemes and further discussion of this hypothesis below). One possible angstrom-level change is the cumulative stacking of phenyl groups inside the polymer due to π-π stacking and van der Waals forces over time. In order to evaluate this hypothesis, the effective number of binding sites and kinetic adsorption-desorption constants were calculated and analyzed.

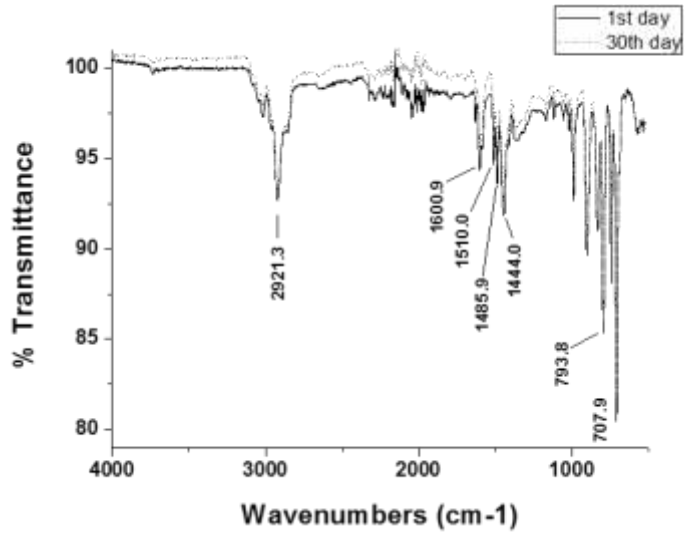

Figure 2.6 FTIR spectra of MIP on the 1st and 30th day after synthesis

3.4 Binding Kinetic Analysis

3.4.1 Adsorption Reaction Kinetic Analysis

Fig. 2.7 shows the adsorption-desorption kinetics of 1ppm o-xylene onto a MIP-modified sensor. As it can be observed in Fig. 7, 120 seconds purging VOC-free air did not allow the MIP-modified sensor signal to return to the baseline level recorded before the injection of 1ppm o-xylene, and a quasi-reversible adsorption-desorption profile characterized the kinetic behavior of fresh sensors. On the contrary, for 1-month old sensors, the adsorption-desorption process was reversible, and 120 seconds purging was sufficient to regenerate the binding sites. It is worth noticing that the change in the kinetic profile was evident. The observation was consistent over 100 of MIP-modified sensors studied. The hypothesis will be further elaborated in the next section.

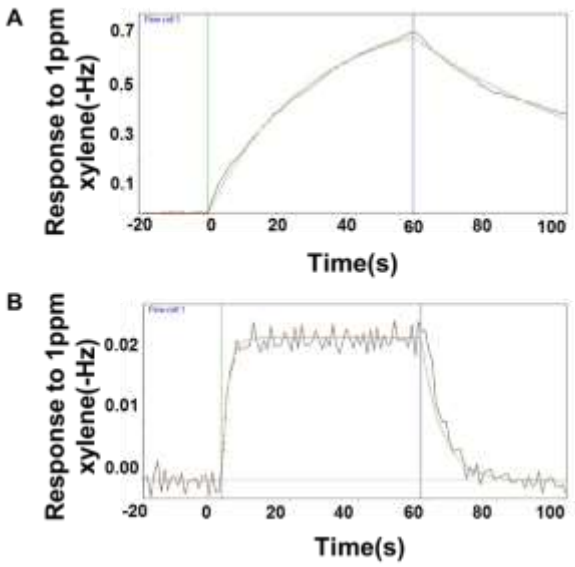

Figure 2.7 Adsorption profile (raw data and smoothed fitting curve) to 1ppm xylene on the first day and 30th day (B) after the MIP-modified QTF sensor is prepared. Time = 0s indicates the injection of the analyte for 60 sec. followed by purging with air.

3.4.2 Total Binding Site Analysis

During polymer synthesis, we use divinylbenzene as both the functional monomer and cross linker, and o-xylene as both the template and solvent. The mole fraction of divinylbenzene and o-xylene is 3:1. The reaction was achieved in a hermetic container and no solvent or segregated phases were observed. Assuming a 100% conversion during synthesis, the theoretical number of binding sites was calculated, together with the actual total number of binding sites, which was extracted from the experimental maximum response of the MIP-modified sensor as follows:

$$[B_0] = \frac{1}{3} * \frac{m}{M_{DVB}} * N_A \qquad 2\text{-}3$$

$$[B_a] = \frac{R_{max}}{M_{xylene}} * N_A \qquad 2\text{-}4$$

where: $[B_0]$ is the theoretical number of binding sites, m is the actual mass of polymer after extraction of solvent (o-xylene) trapped in the binding cavities, M_{DVB} is the molecular weight of divinylbenzene, and N_A is Avogadro's constant. $[B_a]$ is the actual number of binding sites that can be used in detection, R_{max} is the maximum actual response of the sensor obtained from experiment, and M_{xylene} is the molecular weight of o-xylene. Table 2.2 summarizes the results for the number of binding sites at different polymer age. On the first day after QTF sensor was coated with MIP, the percentage of binding sites occupied was 64.5% of the theoretical number of binding sites. After a month, the percentage of binding sites that could be occupied decreased to ~20% of initial value.

Table 2.2 Calculation of binding sites for MIP on the 1st and 30th day after synthesis

	1st day	**30th day**
Coating mass/ng	682	
Theoretical number of binding sites	1.05×10^{15}	
R_{max}/Hz	19.26	5.87
R_{max}/ng	119.4	36.39
Actual maximum number of binding sites	6.77×10^{14}	2.06×10^{14}
Percentage of binding sites occupied at saturation/%	64.5	19.6

As discussed before, calibration curves of MIP-modified QTF sensors on different days were different, and as it is shown in Fig. 2.8, the decrease in response decay within a month under different o-xylene concentrations was also different. Here the response decay is defined as the percentage decrease of response from the first day to 31 days later under different concentration. From Fig. 2.8, it can be observed that the response decrease in QTF sensor is more evident for higher xylene concentrations, and therefore, more binding sites are affected when concentration of the analyte (xylene) is higher. This observation indicates the existence of at least two different types of binding sites in the polymer, and therefore, the adsorption processes could be described as follows (Scheme 2.1): a) Adsorption happens in both inner binding sites located in deep portions of the polymer, so-called cavity adsorption, and onto polymer surface, so-called surface adsorption; b) Adsorption happens mainly on polymer surface and is expected to have a faster desorption kinetic. During the polymer aging, the amount of adsorption cavities inside polymer decreases, leaving the surface adsorption as dominating adsorption process. This can also explain the changes in adsorption-desorption kinetics observed in Fig. 2.7. After aging, response kinetics is more reversible due to adsorption-desorption processes taking place on binding sites located on the polymer surface.

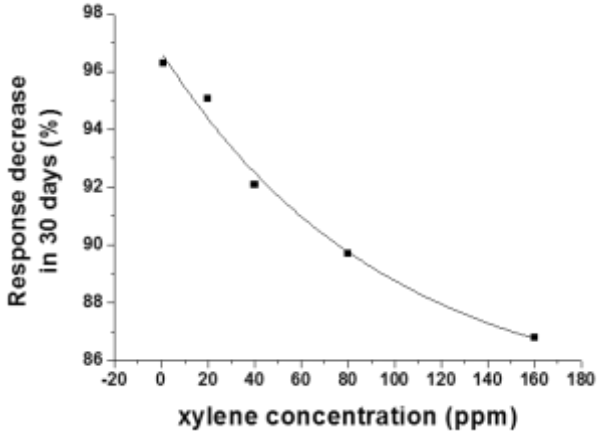

Figure 2.8 Effect of xylene concentration on the response decrease after 30 days. MIP-modified QTF sensor response decrease in 30 days vs. different xylene concentrations.

With low gas analyte concentration, the specific cavity adsorption may be the preferred binding sites. However, the ability of analyte to implement specific cavity adsorption may be impaired at high concentrations, and therefore surface adsorption mechanism dominates. The cavity adsorption mechanism may be reduced as number of sites available reduces as the MIP ages. As we mentioned above, the 3-D polymer conformational change may occur between 3-7 angstrom level, affecting π-π stacking and van der Waals force interaction sites as represented in Scheme 2.2.

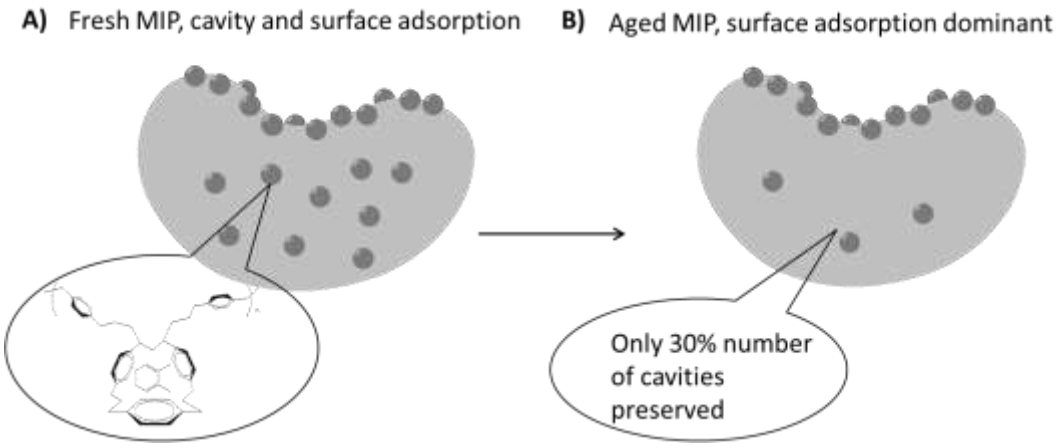

Figure 2.9 Scheme 2.1.(A) Adsorption happens in both specific cavity and on polymer surface for fresh polymer; (B) For aged polymer, surface adsorption is available at low and high xylene concentration, while cavity adsorption dominates more at low xylene concentration

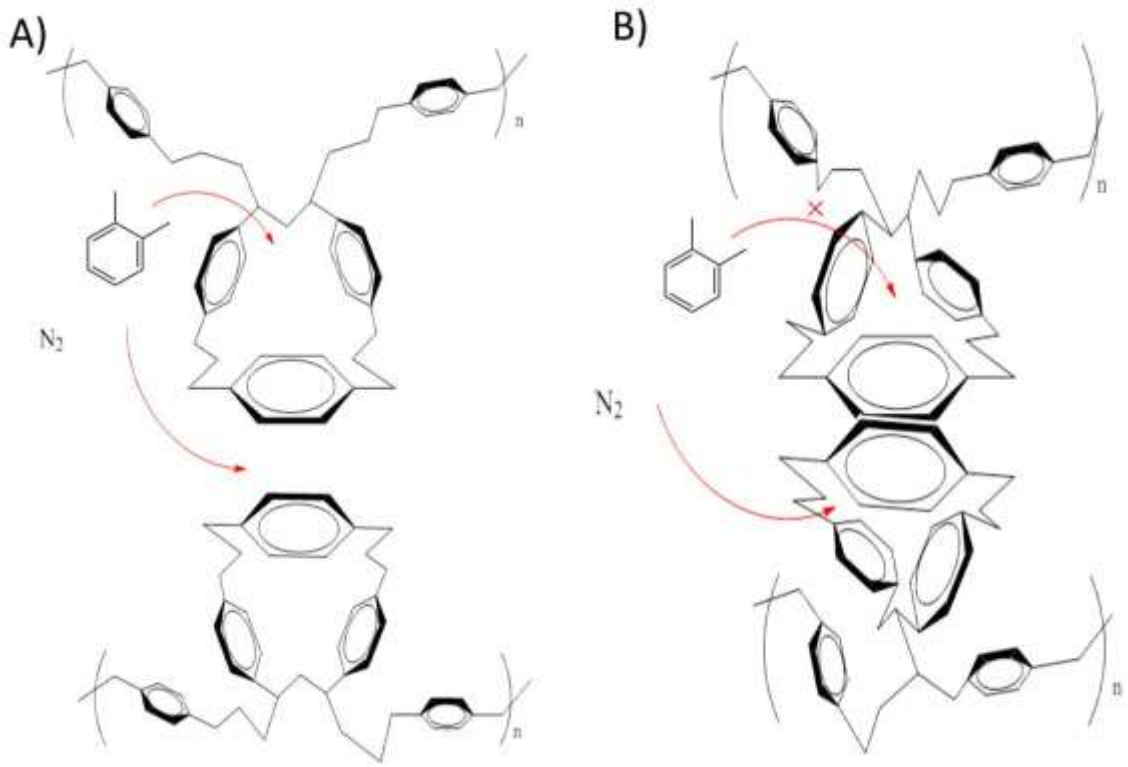

Figure 2.10 Scheme 2.2.Hypothesis scheme for the aging effect on adsorption cavity sites of MIP. (A) Fresh polymer, with abundant cavity adsorption sites, will allow both nitrogen N_2 and xylene to be adsorbed. (B) Aged polymer, with many cavity adsorption sites collapsed at angstrom level, may only adsorb small molecules such as nitrogen N_2. NOTE: The polymer is highly cross-linked with a complicated 3-dimensional net structure. This scheme mainly focuses on showing the change in the cavity.

3.5 Mitigation of Sensitivity Drop

Storage of MIP-modified sensors at -4 °C was used as a mitigation of sensitivity drop. Along this line, it was found that storage of the sensors under low temperature allows achieving sensitivity stabilization for more than four months at ~90% level of the original

sensitivity of Day 1. Details of this portion of the work are not shown here due to further characterization and on-going work. However, the present work provides for the first time evidences of sub-nanoscale instability of MIP materials, which is relevant for MIP-modified QTF sensors, allowing finding better conditions of storage and use of the sensors. Detail description on this improvement will be shown in the next chapter.

It is worthy to mention that nanomaterials have the advantage of high sensitivity due to its high surface area, and high availability of active binding sites compared to their peers in micrometer scales. However, special emphasis needs to be paid to the fact that nanomaterials may possibly be unstable at storage conditions or operational environments [51]. For example, it has been demonstrated that under different temperatures, nanomaterials behave differently [51]. For instance, S.Y. Gao, et.al. [52] and M.L. Williams, et.al [53]. showed that for a single layer of polymer film, the thinner the film, the lower its glass transition temperature, T_g. Glass transition temperatures may be in the range of room operational temperatures for nanomaterials, and therefore attention should be paid to this variable as a potential cause of nanomaterials' structural changes.

4. Conclusion

In this chapter, we explored aging effect of the MIP in connection to its gas adsorption capability, using a MIP-modified QTF sensor located inside a recently developed personal wearable wireless VOC device. SEM, BET, and FTIR characterizations were performed to investigate the change of polymer over time. In parallel, the binding kinetics of the polymer was studied. The characterization study based on SEM, BET, FTIR, and adsorption-desorption analysis in connection to

calculation of binding sites showed that spatial structure change may cause decay in the MIP sensor sensitivity. Furthermore, calculation of number of binding sites availability from different aged MIP indicated there may be a 3-D structural change that impairs the access of analyte molecules to binding sites when the polymer is aged at room temperature conditions.

CHAPTER 3

On the Stability Improvement and Adsorption Thermodynamic Analysis -- A Quartz Tuning Fork Based Sensor for Volatile Organic Compounds (VOCs) Detection

ABSTRACT

A volatile organic compounds (VOCs) sensor based on molecularly imprinted polymer (MIP) and polystyrene mixture modified quartz tuning fork (QTF) has been developed. In this chapter, the stability of the modified sensor has been evaluated. Temperature effect on the adsorption mechanism of target Volatile Organic Compounds (VOCs), such as o-xylene, has been studied. All measurements were carried out in the temperature range of 6-40 ℃. The thermodynamic analysis was carried out from Langmuir model fitted adsorption isotherms. For a freshly modified QTF sensor, the adsorption response increases with rising temperature, while an opposite behavior was observed on an aged QTF sensor. Results show that the adsorption reaction changed from endothermic to exothermic.

1. Introduction

Molecularly imprinted polymer (MIP), a synthetic polymer with specific cavities designed for target molecules, is very often used as selective tools in analytical techniques [54]. Molecular imprinting of synthetic polymers is a process where functional and cross-linking monomers are co-polymerized in the presence of the target analyte (the imprinting molecule), which acts as a molecular template [55]. The template is extracted afterwards, leaving a specific complementary cavity. The highly selective affinity to target analyte makes it attractive in many applications. Research of MIP applications in solid-phase extraction [56, 57], binding assays [58] and sensors [56, 59, 60]have been reported.

A volatile organic compounds (VOCs) sensor based on molecularly imprinted polymer (MIP) modified quartz tuning fork (QTF) has been developed. As described in chapter 2, the polymer is synthesized using o-xylene as a template. It has selective affinity to major hydrocarbon pollutants under many scenarios. Comparing to traditional VOC detection methods, the QTF sensors modified with MIP detect VOC in real-time selectively, and with fast response and high sensitivity. The cost of the sensors and nature of the polymer synthesis also make it a low-cost sensing system. The MIP-modified QTF sensors have been integrated in the wearable wireless gas monitor for VOC detection. Studies in our laboratory and field tests have been performed to validate the specifications of VOC gas monitor based on QTF sensors [25, 33, 61]. This VOC gas monitor has shown the ability to provide timely response to VOCs exposure level, helping to identify potential health risks [62, 63].

As vapor pressure of gas analytes increases with rising temperature, the interaction between gas and solid phase will also change. Thermal and chemical stability of MIPs has been reported before [35, 61], however, there are not many studies about temperature effect on adsorption mechanism of this polymer.

In this chapter, the sensor reproducibility in a scale up fabrication process is studied to ensure the practical application. To overcome the sensitivity decrease discussed in previous publication, polystyrene is added into the sensing material. And this improves the sensor stability over time. The temperature influence on the gas-solid adsorption in the sensing system is studied. The evaluation ranges from 6-39 ℃, which is a common environmental temperature range. Tests are based on the VOCs monitor presented in chapter 2. According to Van't Hoff equation [64], the entropy and enthalpy of the adsorption have been analyzed. This chapter contains preliminary exploration on thermal stability of the sensors after the aging treatment in chapter 2.

2. Methods

2.1 Sensing Mechanism [63]

The sensing mechanism for VOC by our gas monitor is mainly divided into three steps (Fig. 3.1a): 1) Sample collection: The air sample firstly goes through a purging channel for 2 minutes (purging period), where a filter adsorbs particles and VOC interferences to generate a clean air flow, which defines a stable baseline. Then, the flow is switched to a sampling channel for 1 minute (sampling period), where a different filter is used to remove particles only. This generates a particle-free air sample for testing.

Therefore, the total testing cycle involves 2-min purging and 1-min sampling, and it takes a total of 3 minutes. During the entire testing cycle, the sample passes through a dew line to avoid humidity interference. 2) Frequency recording: The MIP-modified QTF is a mass sensitive resonator. The resonant frequency changes between the purging and sampling periods are monitored, and the maximum frequency change is recorded to determine the sensor mass change. This mass change is proportional to the VOC concentration in gas phase. In this paper, the response of the MIP-modified QTF sensor is defined as QTF resonant frequency change. 3) Data transmission: The real-time frequency change of the MIP-modified QTF sensor is transmitted from the VOC gas monitor via Bluetooth® to a smartphone or tablet. With pre-defined correction factors obtained from a sensor QR code (see below), the QTF sensor data is processed in an application located at the smartphone or tablet. Fig. 3.1b) shows a schematic representation of the protocol used for the VOC gas monitor, including pictures of QR code scanning, the gas monitor, user interface, and application.

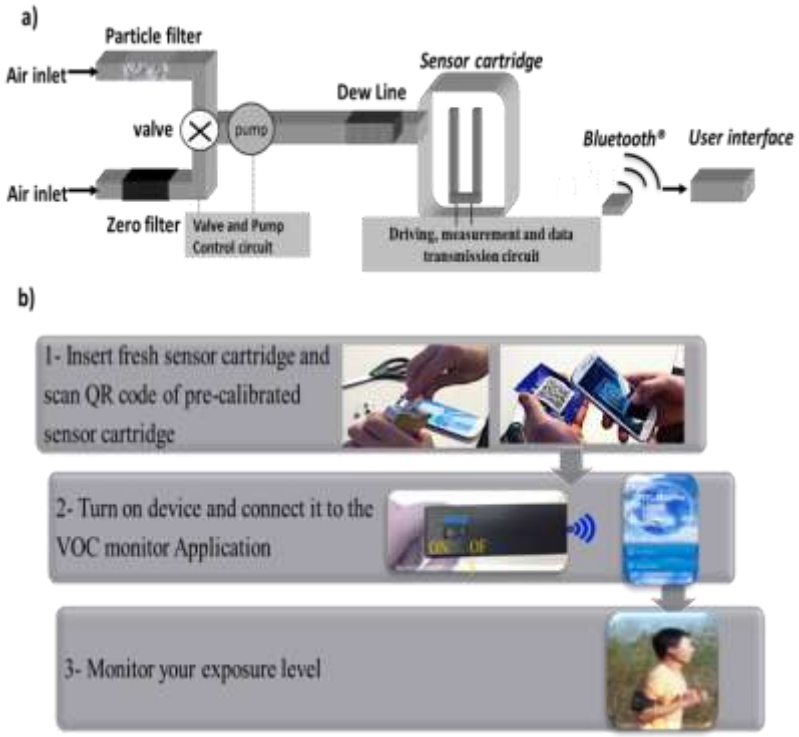

Figure 3.1 Schematic and sensing protocol of the VOC monitor a) Schematic representation of the VOC gas monitor. b) Protocol created for easy and user-friendly use of the VOC gas monitor, including: 1- QR code, 2- Monitor (device) communication with user interface (app in a phone or tablet), 3- Wearing during use.

2.2 Mitigation of Sensitivity Drop On Aged QTF Sensors

As presented in Chapter 2, an aging effect of the MIP modified QTF sensor was observed in terms of sensor sensitivity. The sensitivity dropped more than 90% seven days after the modification. To overcome this issue, polystyrene (from Sigma Aldrich, M_w ~ 35,000) is introduced as "organic glue" to avoid conformational collapse inside the polymer by mixing MIP with polystyrene (PS) with a mass ratio of 19:16.

The stability improvement was evaluated on MIP and PS mixture coated QTF sensors in the following procedure: 1) Two batches of QTF sensors (200 sensors for each batch) were modified with the mixture; 2) Each modified sensor was marked, packed and sealed in a laminated bag (Fig. 1) after their initial response measurement; 3) All sensors were stored in -4℃ freezer; 4) One QTF sensor from each batch was randomly picked out for one time test with 40ppm o-xylene under room temperature. Each sensor was used for only one test to exclude potential impact due to the measurement. The test frequency was one week per test in the first four months and two week per test for eight months after that.

2.3 Temperature Effect Investigation

O-Xylene was chosen as a calibration gas and vapor sample was generated from liquid o-xylene. All calibration tests were done in a sealed box, where sample concentration and ambient temperature could be controlled. A thermistor was implemented inside the device to monitor the environmental temperature. The sensitivity of the MIP-modified QTF sensor was calibrated, using six different o-xylene concentrations over three different temperatures (6℃, 25℃, 39℃). Langmuir adsorption isotherm was applied in curve fitting (Equation 2-1 and 2-2).

2.4 Thermal Stability Validation

As a sensor operating under free-living conditions, the MIP-modified QTF sensor's performance may be influenced not only by environmental temperature sensing conditions, but also by conditions during shipping. From our experience, higher

temperature exposure may induce a decrease in sensitivity, and therefore, temperature during shipping may be important to quality control. To maintain sensor sensitivity, we determined that it is important to use cold packs and boxes with good thermal insulation property to pack the sensors. To validate this packing method, we simulated a 2-day shipping condition, during which the sensors were kept at 25 ℃ for 40 hours and 40 ℃ for 8 hours. Along this line, the sensitivity of the packed MIP-modified QTF sensor was measured before and after the exposure to the simulated 2-day shipping condition. A control group, which did not have any thermal insulating protection during the two days, was also tested for comparative purpose.

2.5 Thermodynamic Analysis of the Adsorption Process

Another factor that may impact on sensor sensitivity is temperature. Under different temperature, gas sample has different vapor pressure, and adsorption kinetics is also changing. Hence, it is necessary to study on the temperature effect on the sensors. In combination with the aging effect talked above, the temperature effect on freshly modified QTF sensor and aged modified QTF sensor was also studied.

O-xylene was chosen as calibration gas and vapor sample was generated from liquid o-xylene. All calibration tests were done in a sealed glovebox, where sample concentration and ambient temperature could be controlled. A thermistor was implemented inside the device to monitor the environmental temperature. The sensitivity of the sensor was calibrated, using six different o-xylene concentrations over three different temperatures (279K, 297K, 312K). The testing sequence was from low

temperature to high temperature. Sample concentrations were generated from liquid o-xylene and controlled around 0ppm, 10ppm, 20ppm, 50ppm and 100ppm (from low concentration to high concentration). The accurate concentration was measured by a photo-ionization detector from RAE systems (RAE by Honeywell®). Langmuir adsorption isotherm was applied in curve fitting.

In this section, four groups of modified QTF sensors were tested: Group 1 – Freshly MIP modified QTF sensor; Group 2 – Freshly MIP and PS mixture modified QTF sensor; Group 3 – Aged MIP modified QTF sensor; Group 4 – Aged MIP and PS mixture modified QTF sensor. Three sensors from each group were tested. The fresh condition refers that test was done one day after the QTF sensors were modified. And the aged condition refers that test was done seven days after the QTF sensors were modified, during which the sensors were kept in a close environment under 297K.

2.6 Van't Hoff Equation

Under standard conditions, the Van't Hoff equation is [65]

$$\frac{dlnK_{eq}}{dT} = \frac{\Delta H^{\ominus}}{RT^2} \qquad 3\text{-}1$$

where R is the ideal gas constant, $\Delta H^{\ominus}$ is reaction enthalpy, K_{eq} is equilibrium constant and T is absolute temperature.

Assuming reaction enthalpy is constant, the equation could be derived to estimate the relationship between temperature and equilibrium constant [66]

$$lnK_{eq} = -\frac{\Delta H^{\ominus}}{RT} + \frac{\Delta S^{\ominus}}{R} \qquad 3\text{-}2$$

in which the definition of Gibbs free energy

$$\Delta G^{\ominus} = -RTlnK_{eq} \qquad 3\text{-}3$$

is also applied.

Thus, a linear relationship between lnK_{eq} and 1/T could be plotted. When the slope ($-\frac{\Delta H^{\ominus}}{R}$) is positive, the reaction is exothermic. Likewise, the negative slope indicates an endothermic reaction.

3. Results and Discussion

3.1 Sensor Fabrication and Stability

Fig. 3.2 shows the coating mass and response distribution of 200 MIP and PS mixture coated QTF sensors fabricated in one batch. The mass sensitivity of the QTF sensor used here is 66 ng/Hz. Thus the loading mass of mixture on the QTF prong is presented in terms of Hz.

As shown in Fig. 3.2, the distribution of coating mass and response to 40 ppm o-xylene has standard deviation within 10.5%, which indicates the fabrication process reproducible. And this also proves the validity of stability test (see below).

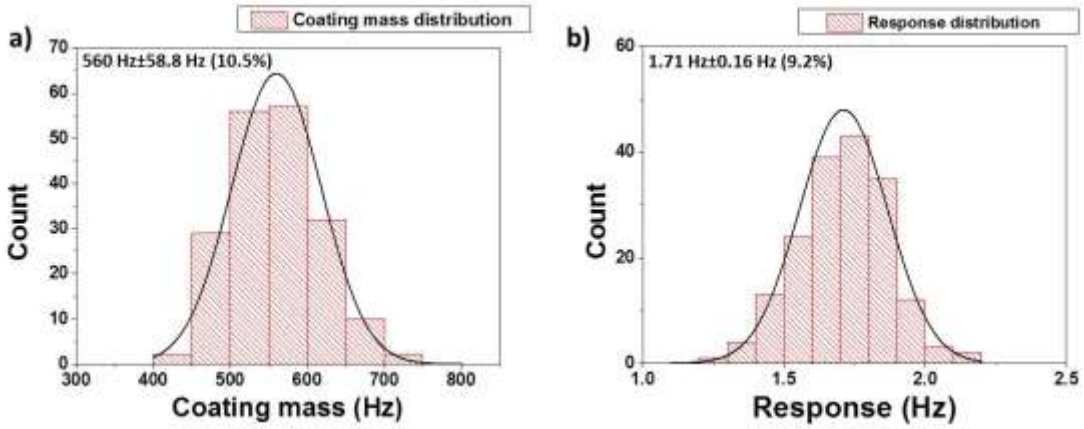

Figure 3.2Reproducibility of sensor fabrication protocol on 200 QTF sensors. a) Distribution of coating mass on QTF; b) Distribution of reponse to 40ppm xylene.

As mentioned in experimental part, previous chapter described and characterized an aging effect happened on the QTF sensor: on QTF sensors modified with MIP only, the response to same concentration of o-xylene vapor will drop 90% in seven days after it's fabricated. Fig. 3.3a) shows the response degradation on QTF sensors coated with MIP only. The over 90% lost in response makes the sensors lack of sensitivity thus it is no longer useful. This is not applicable for real world scenario.

Adding PS into the sensing material mitigates this response decay. Fig. 3.3b) shows the improvement of sensor stability with addition of PS. The sensors remained 60%-70% of its initial sensitivity 4 months after they were fabricated. Even after one year, the response still remains over 50%. And also, the reproducible linear curve fitting between the logarithmic of time and sensor response to 40ppm o-xylene can be used to predict the response of the sensors.

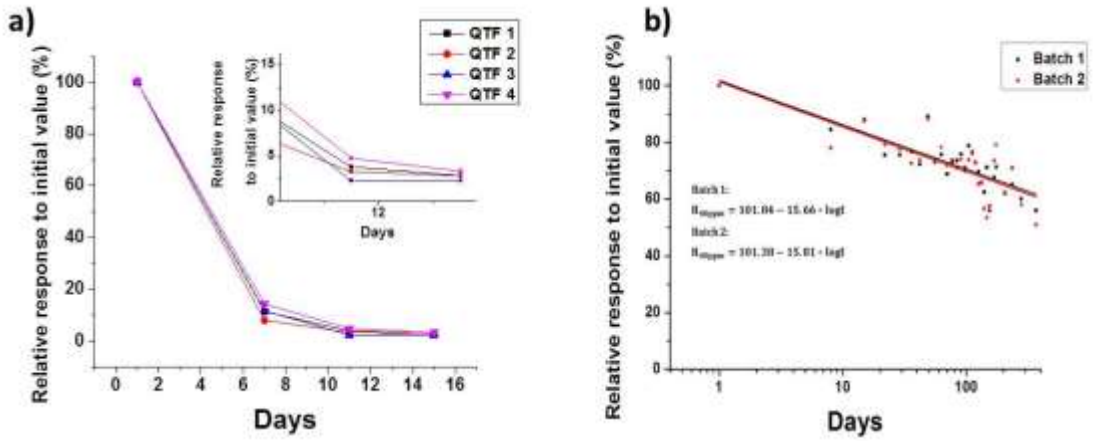

Figure 3.3 Stability test on QTF sensors. a) QTF sensors modified with MIP only; b) QTF sensors modified with MIP and PS mixture

The above comparison shows the enhancement of sensor stability by mixing PS with MIP as sensing material. Possible explanation is that PS strings support the inner structure of MIP and prevent it from collapsing. This is the first time that a method to enhance the time stability of MIP has been reported.

3.2 Temperature Effect

3.2.1 Fresh QTF Sensors

In this test, group 1 (MIP only) and 2 (MIP+PS mixture) QTF sensors were tested one day after they were modified. The adsorption response is normalized with coating mass.

Fig. 3.4 shows the calibration curves of a freshly modified QTF sensor under different temperature. Langmuir fitting is applied to all three curves. Fig. 3a) shows that

MIP QTF sensor response decreases with temperature increment. Both R_{max} and K_D decrease with rising temperature. An opposite performance is observed on MIP+PS QTF sensor, as shown in Fig. 3 b): both R_{max} and K_D increase with temperature increment.

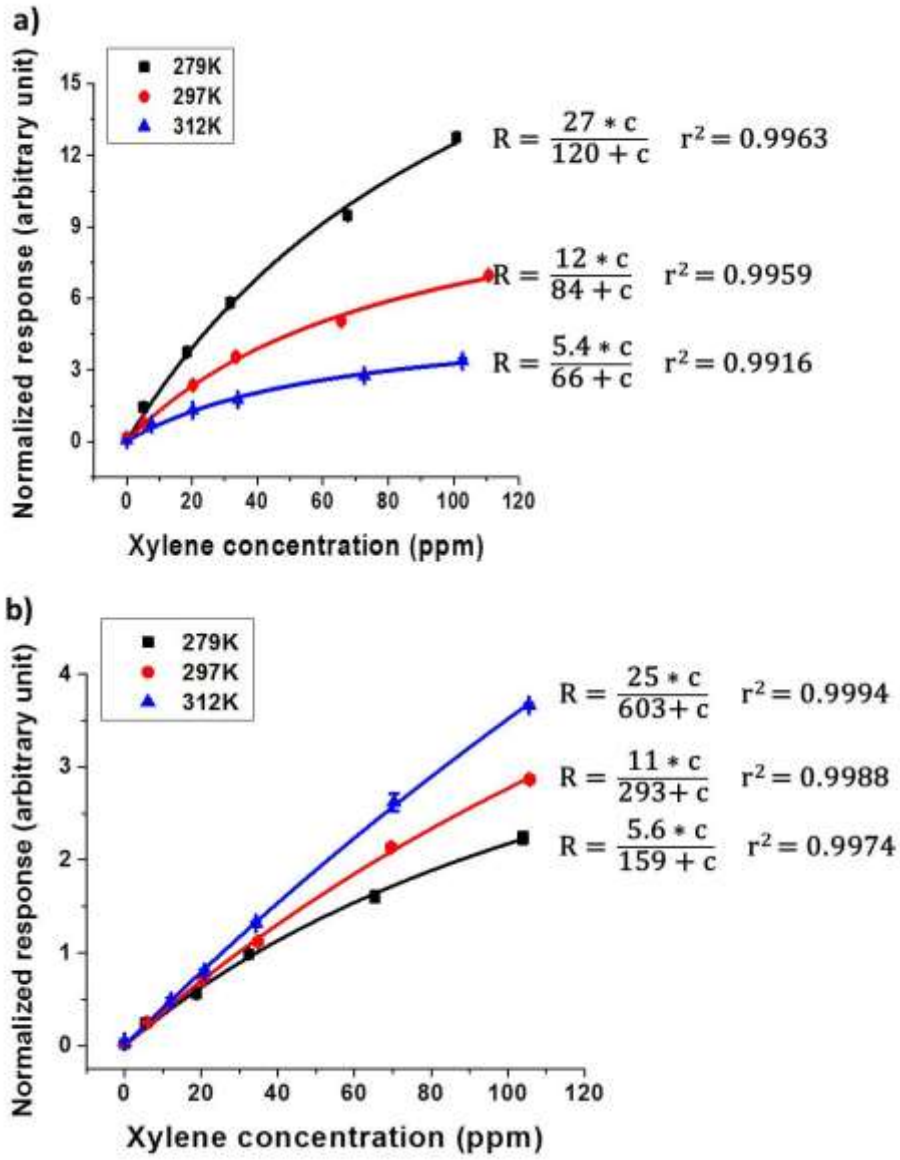

Figure 3.4 Fresh QTF sensor calibrations under different temperature. a) Response on MIP modified QTF sensors; b) Response on MIP+PS modified QTF sensors

3.2.2 Aged QTF Sensors

The above observations happened when the QTF sensors were in fresh condition. In this section, we tested QTF sensors that had been stored at 297K for seven days after the modification (Group 3 and 4). During the storing time, the QTF sensors were kept in close environment to prevent other interference.

Fig. 3.5 shows the results. On MIP modified QTF sensor (Fig. 3.5a), the effect from temperature has similar trend as freshly modified QTF sensor. Both R_{max} and K_D increase with temperature decrement, although the response drops 90%.

Further analysis will be shown in next section.

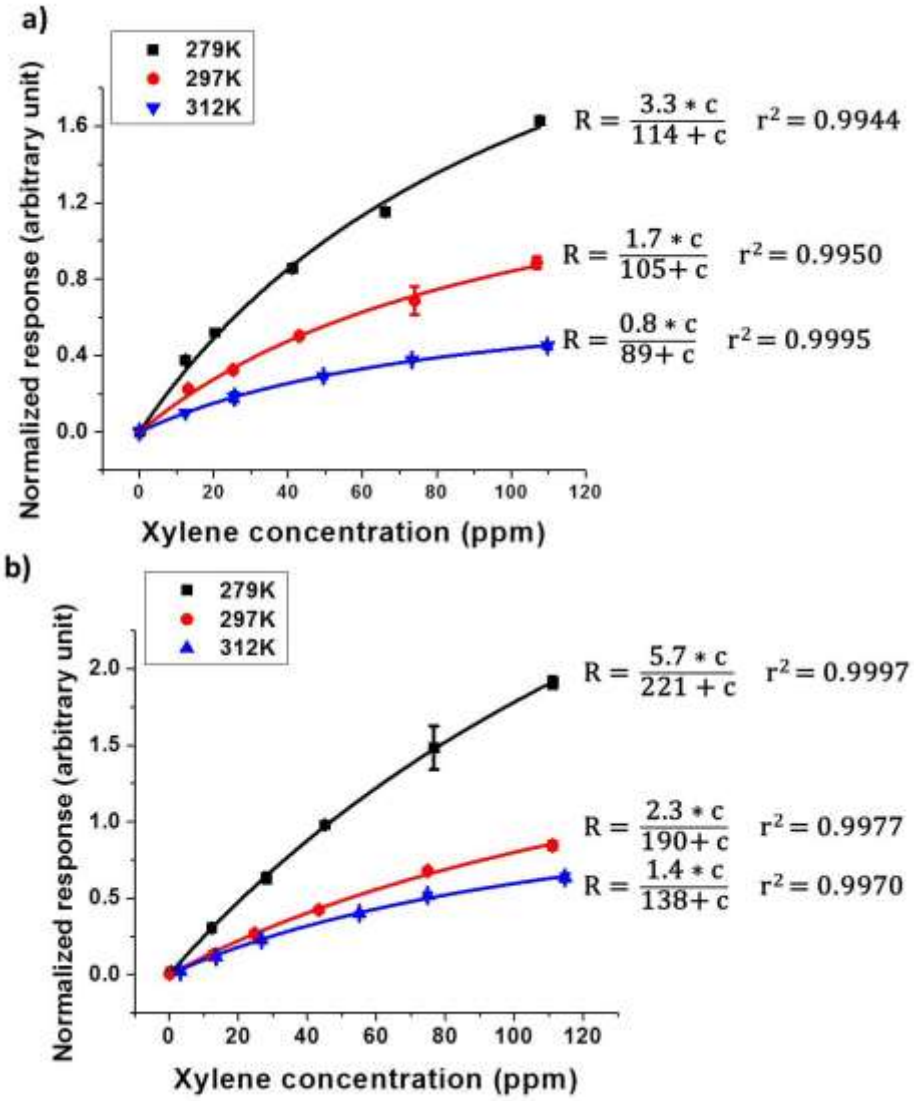

Figure 3.5 Aged QTF sensor calibrations under different temperature. a) Response on MIP modified QTF sensors; b) Response on MIP+PS modified QTF sensors

3.3 Thermodynamic Analysis

As for MIP and PS mixture modified QTF sensor, the result is shown in Fig. 3.5b). Under same o-xylene concentration, the sensor response, R_{max} and K_D decreases with rising temperature. This result demonstrates that response behavior under different temperature reverses on MIP and PS mixture modified QTF sensors over time. As discussed in chapter 2, we proposed that the 3-dimensional structure change in polymer would induce the response degradation. The adsorption could be affected by many factors such as reaction rate (Arrhenius equation [67])

$$k = Ae^{-E_a/(RT)} \qquad 3\text{-}4$$

where k is the reaction rate constant, T is absolute temperature, A is a pre-exponential factor (constant), E_a is the activation energy of the reaction and R is gas constant. Given A, R and E_a positive, the adsorption rate constant will increase with temperature increment.

According to Van't Hoff equation, the relationship between reaction equilibrium constant K_D and temperature could be estimated, as shown in Fig. 3.4.

As an estimate of the adsorption, two graphs in Fig. 3.6 show the $\ln K_D$ VS 1/T of fresh (a) and aged (b) QTF sensors. Although three points are not adequate to quantitatively analyze the reaction energy, it already provides evidence of the mechanism change in adsorption.

Another explanation for the adsorption change over time is the intrinsic polymer change. As discussed in previous publication, we proposed that the 3-dimensional structure change in polymer would induce the response degradation. This change in structure will effect on adsorption in test.

From the calibration data, the relationship between reaction equilibrium constant K_D and temperature could be plotted (expressed in Van't Hoff Equation), as shown in Fig. 3.6.

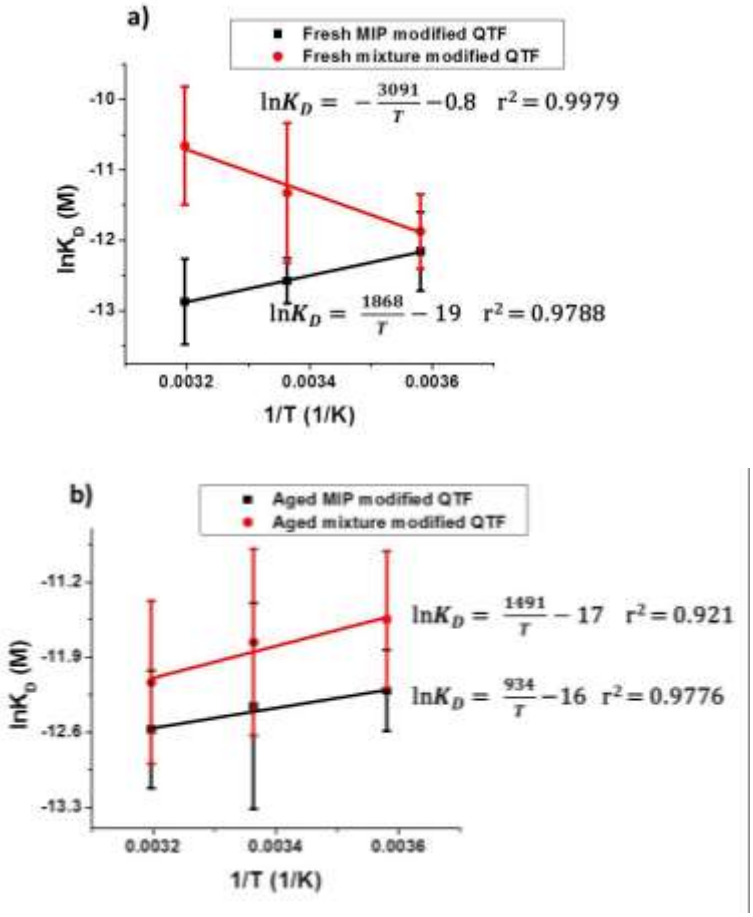

Figure 3.6 Van't Hoff plot of: a) Fresh QTF sensor; b) Aged QTF sensor

The summary of energy calculation from Van't Hoff equation is shown in Table 3.1.

Table 3.1 Energy analysis on adsorption

	Fresh MIP modified	**Fresh mixture modified**	**Aged MIP modified**	**Aged mixture modified**
ΔH/ kJ	-15.53	25.7	-7.76	-12.40
ΔS/J·K	6.82	156.80	-129.28	-140.17

From the stability plot, it could be concluded that MIP modified QTF sensors sensitivity significantly faster than mixture modified QTF sensors. This could also be expressed as that the polymer structure is reaching a steady state over time. In the linear fitted plots shown in Fig. 5, the positive slope ($-\frac{\Delta H^{\ominus}}{R}$) indicates an endothermic reaction, while the negative slope demonstrates the adsorption changed into exothermic. By releasing energy in an exothermic reaction, the potential energy of reactants will decrease when it became products. And for endothermic reaction, the potential energy elevates from reactants to products. From Table 1, the enthalpy change (ΔH) of MIP modified QTF sensors decreases after they are aged, indicating that the aged state is closer to the product energy level. The ΔH of mixture modified QTF sensors changed from positive to negative, which demonstrate the adsorption reaction changed from endothermic to exothermic.

The MIP structure has a trend of relaxing to a lower energy level state. This result fits the expectation of adding PS into the sensing material to improve the stability issue: PS will slow down MIP inner structure from collapsing, which makes lifetime of the

sensor much longer and useful. It is possible that for MIP modified QTF sensor, the material relaxing is faster than one day. Thus the adsorption reaction already reached to be exothermic during the test. However, for the mixture modified QTF sensors, the material relaxation time is prolonged, which is the observation of this test.

This is the first time reported that mixing PS with MIP will alter the adsorption reaction from endothermic to exothermic. It is meaningful in applying MIP into more real world applications.

3.4 Thermal Stability Test Results

As a product, accurate sensitivity needs to be ensured under different scenarios. One of the big issues for a lot of chemical and bio specimen transportation is that they may degrade after staying at high temperature. As a thermal sensitive material, the reproducible response of the QTF sensors needs to be ensured. A simulated shipping condition is created to validate its thermal stability.

Fig. 3.7 shows the effect of simulated 2-day shipping condition on the MIP-modified QTF sensor sensitivity as explained in the experimental sections. Fig. 3.7a) considers the case of the sensor with no thermal control (QTF 1 & QTF 2), while Fig. 3.7b) shows the case when the thermal control with cold pack and thermal insulating box were applied (QTF 3 & QTF 4). The sensitivity of the sensors was evaluated at 25 ℃. It is worth noticing that the effect of thermal insulation of the sensors is necessary to keep the sensitivity of the sensor between 97-100% of the original sensitivity, and therefore, it is an important factor from practical standpoint to ensure sensor sensitivity during transit.

Results not shown here also indicated the need of keeping the sensors stored at low temperature (-10 ℃) to preserve the original sensitivity over extended storage period.

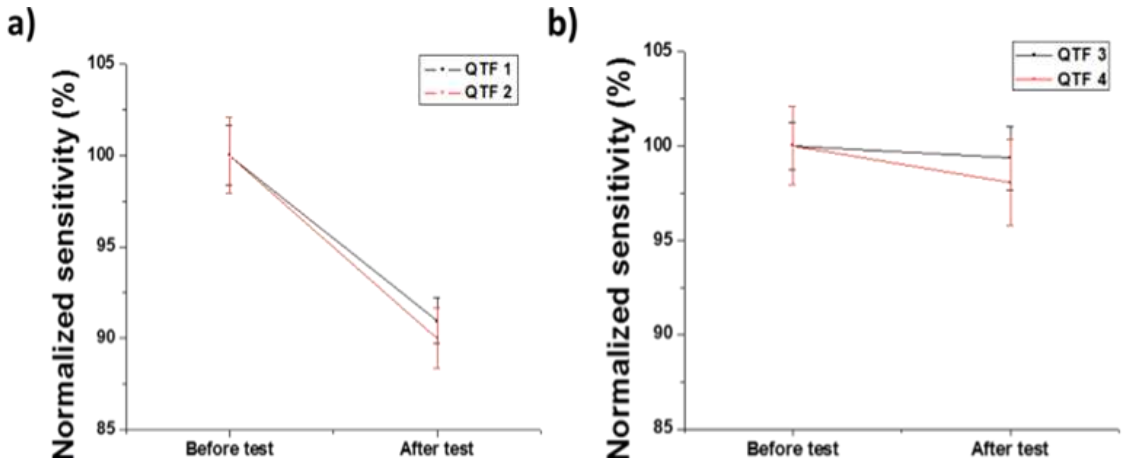

Figure 3.7 Effect of simulated 2-day shipping condition on the MIP-modified QTF sensor for a) No thermal control for the sensors; b) Thermal control with cold pack and thermal insulating box.

4. Conclusion

In this paper, stability of a QTF based gas sensor for environmental VOCs detection has been tested. By mixing MIP and PS together, the stability has been improved and the calibration under different temperature on fresh/aged MIP modified or MIP and PS mixture modified QTF sensor is presented. Results show that there is a significant response difference under different temperature between a freshly modified sensor and an aged sensor. Thermodynamic analysis on the calibration data shows that adsorption reaction on the mixture modified QTF sensors goes through a transforming

from endothermic reaction to exothermic reaction. This is the first time that this kind of behavior has been reported. It is of great significance in MIP applications. To ensure the themal stability, a 2-day shipping condition is simulated. As expected, the QTF sensors can maintain over 90% sensitivity when it's packed in a gel cold pack for two days.

CHAPTER 4

A Novel Wearable Wireless Device for Hydrocarbons Detection and Its Fabrication

ABSTRACT

A novel portable wireless volatile organic compound (VOC) monitoring device with disposable sensors is presented. The device is miniaturized, light, easy-to-use, and cost-effective. Different field tests have been carried out to identify the operational, analytical, and functional performance of the device and its sensors. The device was compared to a commercial photo-ionization detector, gas chromatography-mass spectrometry, and carbon monoxide detector. In addition, environmental operational conditions, such as barometric change, temperature change and wind conditions were also tested to evaluate the device performance. The multiple comparisons and tests indicate that the proposed VOC device is adequate to characterize personal exposure in many real-world scenarios and is applicable for personal daily use.

1. Introduction

Volatile organic compounds (VOCs) are organic chemicals emitted from anthropogenic and biogenic sources with significant vapor pressure [1]. Examples of VOCs are aromatic hydrocarbons, such as benzene, xylene, and alkanes such as hexane [68]. According to the United States Environmental Protection Agency (EPA), VOCs are among the major pollutants for indoor and outdoor air quality since they are emitted from furniture, appliances, and construction materials [69] as well as combustion of fuels (cars and trucks) [70]. Harmful VOCs typically are not acutely toxic, but have compounding long-term health effects [28]. Therefore, there is a need of determining real-time personal exposure concentrations. Many works have reported qualitative and quantitative analyses of indoor and outdoor VOC concentrations [71-73]. Popular methods such as photo-ionization detection [17] and gas chromatography (GC)-mass spectrometry (MS) [74] have been developed. In addition, other techniques such as thermal conductivity (TCD) [11], flame ionization (FID) [13], and differential mobility (DMD) [12] have been established to support detection with GC.

Quartz tuning forks (QTFs) are highly mass sensitive piezo-electronic resonators commonly used in watches for timing purposes and as biosensors for sensing applications [26]. By taking advantage of their small size and cheap cost, QTFs have been used as sensing elements for gas detection [75]. Our group has developed a wearable wireless monitor based on QTF sensors [32, 33, 42]. A film of molecularly imprinted polymer (MIP), which is selective and sensitive to target VOCs, has been applied on the surface of a QTF sensor. The MIP is a highly crosslinked polymer that is formed with a template

molecule that is extracted afterwards, leaving selective cavities to create chemical affinity to molecules with similar structure [61]. When target VOCs molecules are adsorbed onto the polymer, a change in resonant frequency (induced from loaded mass change on the QTF sensor) is detected.

Compared to traditional detection methods, which are usually bulky or expensive, the QTF sensing mechanism gives the opportunity to develop non-intrusive, fast response, high sensitivity, and portable devices for personal VOC exposure detection. Studies in lab and field tests have been done to validate the specifications of a QTF-based VOC device [31]. The VOC device has shown the ability to provide timely response to VOCs exposure level, helping to identify potential health risks [62]. However, previous VOC device had an embedded QTF sensor inside the device and required special calibration protocols in the laboratory, which made it dependent on operator expertise. In addition, although the previous VOC device was relatively smaller compared to portable Photo Ionization Detectors, it was still too bulky to comfortably wear it for long periods of time. Furthermore, the VOC device required strict operation procedure to be followed, making operation less user-friendly.

In this chapter, a new model of a VOC-sensing device based on QTF sensors is presented. Industrial, mass production, and design engineering work have been thoroughly performed to produce an end-user friendly VOC device as follows: (1) In order to avoid laboratory calibration procedures dependent on expertise, a replaceable pre-calibrated sensor cartridge has been created. (2) In order to improve wearability and encourage more user compliance (i.e., device wear-time), a two times smaller volume

VOC device has been designed and mass-produced, including highly integrated components. (3) In order to produce an easy-to use device, a new user interface with embedded guidance has been created as a mobile application in a phone or tablet. It is worthy to mention that in many cases, a fully functional VOC-sensing device for real-world conditions is not trivial since stability of the materials, robustness of the sensor, and optimal device design must be met. Many lab-bench devices cannot reach this specific state and never become commercialized. In fact, there is a big gap between the number of publications in VOC-sensing devices published in the last 16 years (~34,000 publications) and the very few VOC monitors that are actually commercially available shows the difficulty of successfully implementing VOC-sensing devices in real applications. In order to validate the analytical, functional, and field-testing usability of the new VOC device presented in this publication, the performance of the VOC device is compared with existing commercial monitors such as a photo-ionization detector, gas chromatography-mass spectrometry, and carbon monoxide detector. In addition, environmental operational conditions, such as barometric pressure, temperature inversion, wind speed, and wind direction are also used to interrogate if the new VOC device's performance is as expected. The multiple comparisons and tests indicate that the new wearable VOC device is suitable in characterizing personal exposure in real-world scenarios and is applicable for daily use. The progress reported here allows the present VOC device to reach future commercialization venues.

2. Materials and Methods

2.1 Device Sensing Mechanism

The personal VOC device based on QTF sensors consists of four functions: (1) Collection and delivery: the air sample is collected and delivered via an alternating channel valve-activated mechanism with a purging channel, delivering a VOC-free baseline for 120 s and a sampling channel, delivering the gas sample to analyze for 60 s. Environment hydrocarbons are tested through the sampling channel. Humidity of air sample is balanced by a Nafion® tube. (2) Sensing and detection: after the air sample is produced, it passes a sensor chamber with a MIP-modified QTF sensor inside, and the sensing signal from the sampling vs. purging channels are compared and assessed. (3) Signal conversion and data transfer: the resonant frequency shift of the MIP-modified QTF sensor is the sensor signal output, which allows detection of gas phase analyte concentration due to the mass loading effect of the adsorption of molecules onto the MIP. (4) Data transmission and signal processing: the differential sensor signal is transmitted to a smart phone via Bluetooth®, where raw signal is captured, and further processed to provide concentration output. Detailed descriptions of the circuit have been provided in a previous publication [31].

2.2 Apparatus

2.2.1 Photo-Ionization Detector (PID)

PID is one of the popular techniques for VOC concentration monitoring. A MiniRAE Lite photo-ionization detector from RAE Systems Inc. (San Jose, CA, USA)

was used for comparison of VOC device performance, and real-time data from the PID monitor was recorded.

2.2.2 Gas Chromatography/Mass Spectrometry (GC-MS)

Field tests at Mammoth Spring, Yellowstone National Park (WY, USA) were performed to validate the selectivity of the VOC device in an environment with high concentration of hydrogen sulfide, H2S. Since H2S does not belong to volatile organic compounds, although it is very common in some environmental scenarios such as petroleum refinery [76], H2S constitutes a major risk of interference for non-selective VOC monitors. To identify the existence of H2S, an air sample was collected and analyzed in a laboratory equipped with a GC-MS system (HP 5890 Gas Chromatograph interfaced to HP 5972 Mass Selective Detector Quadrupole Mass Spectrometer (Santa Clara, CA, USA) and with a Chromosil 330 column, Supelco, Sigma-Aldrich Co. (St. Louis, MO, USA). Prior to use, the GC column was conditioned overnight at 100 ℃ with dry carrier gas (nitrogen) at a flow of 20 mL/min. The gas sample was pre-concentrated in a polydimethylsiloxane coated solid phase micro extraction fiber (SPME) for 1 h, and desorbed from the SPME fiber into the GC at 200 ℃. Selected Ion Monitoring mode was used in the mass spectrometry detector to get a better resolution of results and discrimination from interference. Identification of the analytes was performed using known standards and the mass spectrum library from NIST (AMDIS32 software, Gaithersburg, MD, USA).

2.2.3 Carbon Monoxide Monitor

Carbon monoxide is very common in vehicle exhaust due to the incomplete combustion of gasoline [77]. It is also emitted to the environment along with VOCs, causing pollution. In order to test the correlation of the hydrocarbon concentration detected by the VOC device with carbon monoxide concentration, a commercial carbon monoxide (CO) (monitor Q-Track, Shoreview, MN， USA) was used to monitor carbon monoxide (CO) concentration to compare and correlate with the VOC device, and real-time data from the CO monitor was recorded.

2.2.4 Abbreviations Used Throughout this Work

In this paper, TVOC device stands for total VOC device and HC stands for hydrocarbon. The concentrations stated as part per million (ppm) refer to volume in volume concentrations (ppmV). For total VOC concentration, the unit ppmC indicates volume in volume total carbon concentration.

2.2.5 Field Testing's Subjects

The Institutional Review Board (IRB) from Arizona State University # 1304009100 entitled A Pocket-Sized Device for Personal Exposure Level Assessment was followed. Four subjects wore and used the VOC device. None of them reported discomfort while using it. Furthermore, the subjects felt comfortable with the use of the monitor and found the user interface to be friendly.

3. Results and Discussion

3.1 Device Evaluation

3.1.1 Device Development and Comparison

Figure 4.1a) shows the new version of the VOC device, which is 2.1 times smaller in size than the previous generation device (12.7 cm × 7.6 cm × 3.6 cm). In addition, the new device is four times lighter in weight, making it a truly portable monitor, which is suitable to wear in a cell-phone type armband.

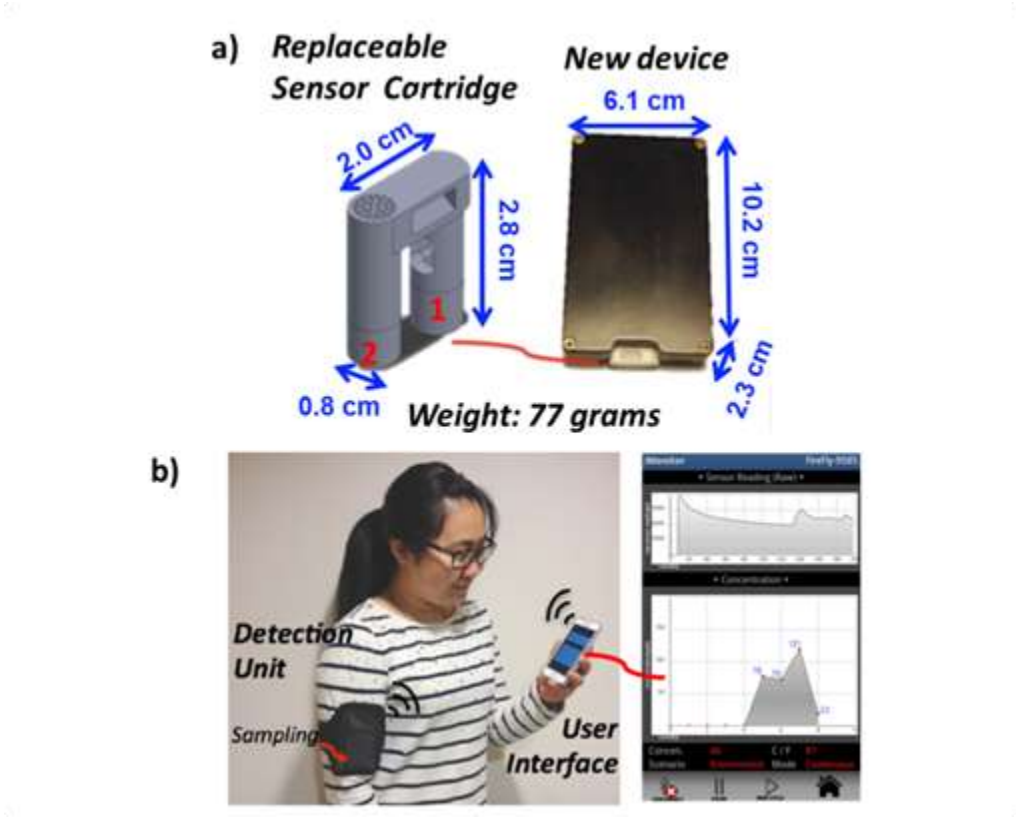

Figure 4.1 Replaceable sensor cartridge and user interface (a) Device dimension and weight; (b) Pictures of sensor components and user interface on a smart phone

As mentioned before, another feature of the new VOC device generation is the replaceable pre-calibrated sensor cartridge for easy use of fresh and calibrated sensors during field studies. The replacement pre-calibrated sensor cartridges (part 1 shown in Figure 4.1a) are used with a QR-coded picture procedure, which is included in a guided protocol in the user interface of the device at the smart phone. In this way, former tedious sensor replacement (opening and closing of the housing), and in-situ gas sensor calibration is avoided by the replacement of the sensor element, and the use of a QR code containing the calibration factor of the "on-spot & ready-to-use" sensor. Each new replaceable sensor cartridge is also equipped with a chemical filter (part 2 shown in Figure 4.1a) for purging channel to ensure fresh filtering efficiency. The sensors have a lifetime of 464 ppmC·h (see Table 4.1, and corresponding reference). A thermistor is also integrated in the flow channel to monitor temperature of the sensing environment, which is necessary for temperature correction of sensitivity (see Supplementary Material). The QR code with pre-calibrated sensor information can guarantee the accuracy of tests for a period of 12+ h of continuous use (see Supplementary Material). The decrease in size and weight of the device and introducing of replaceable sensor make the epidemiology tests with this device more convenient and user friendly (see below).

Figure 4.1b) shows the components of the VOC device system, including the wearable VOC device and a smart phone with the user interface application installed. Figure 1b also shows plots of the real-time sensor signal (upper chart), and the environmental total hydrocarbon concentration (lower chart) in the user interface. The

real-time sensor signal is captured every second and the environmental total hydrocarbon concentration is determined every three minutes.

Table 4.1 summarizes the specifications of the new VOC device with a MIP-modified TF sensor (MIP-TF sensor) for detection of hydrocarbons. The hydrocarbon sensor, as presented here, primarily detects hydrocarbon compounds, including aromatic, alkyl, and chlorinated hydrocarbons, with a measurement range from 2 to 320 ppm xylene equivalent concentrations. In addition, tests performed under different environmental conditions indicated that the device can be operated regularly under a temperature range of 32 ℉ to 113 ℉ (0 ℃ to 45 ℃) and a humidity range of 0 to 95% RH (non-condensing). The accuracy of the sensor, when tested with artificial single hydrocarbon samples (e.g. xylenes), is better than 4% of the measured value.

The lifetime of the sensor is defined as the total amount of time sensors used (in hours) times the hydrocarbon concentration (ppmC) that the sensor has been exposed to, which is monitored by the device. As an example, the current device could be used for 465 hours if it is being exposed to 1 ppmC VOC. The MIP-TF sensors are stored at -18 ℃, which is a common temperature of a home freezer. Sensor shelf time will be discussed below.

In comparison, Table 4.1 also shows the respective specifications from PID. Our device fits daily personal use purpose better in terms of operating easiness and requirements.

Table 4.1 Device Specifications and Comparison with Other Techniques

Techniques	**HC Device**	**PID (Photo Ionization Detector)**
Operating temperature	32 ℉ to 113 ℉ (0 ℃ to 45 ℃)	-4 ºto 122 ºF (-20 ºC to 50 ºC)
Operating humidity range	0 to 95% RH (non-condensing)	0 to 95% RH (non-condensing)
HCs Measurement range	2 ppm to 320 ppm	0.1 ppm to 2000 ppm
HCs accuracy	±4% of measured value or better	±5% of measured value or better
Calibration	Pre-calibrated	With standard Isobutylene cylinder
Response time	Raw Data: 1 second per measurement Calibrated concentration: 3 minutes per data point(adjustable)	2 seconds
Dimensions	4.0 in × 2.4 in × 0.9 in	9.3 in × 3.6 in × 2.9 in
Weight	0.17 lbs	1.75 lbs
Warm up time	< 10 mins	< 10 mins

3.2 Device Calibration, Selectivity of Sensors

Figure 4.2 shows a calibration curve of the new VOC device with a MIP-QTF sensor using the above-described setup. The calibration curve represents the sensor signal frequency change in presence of the sample vs. the absence of the sample (clean air baseline) under different concentrations of gas samples, including 0 ppm (clean air), 7.9 ppm, 15.8 ppm, 36 ppm, 76.5 ppm, and 160 ppm of o-xylene. o-xylene was chosen as

model analyte to evaluate performance due to the abundance in traffic scenarios. The diluted samples were prepared in laminated bags with clean and dry air balance. All air sample concentrations were also monitored using PID as reference. The calibration curve is fitted to Langmuir adsorption isotherm, which is described by a relationship between the sensor response and analyte concentration with a fitting squared-regression coefficients (r^2) close to 1.

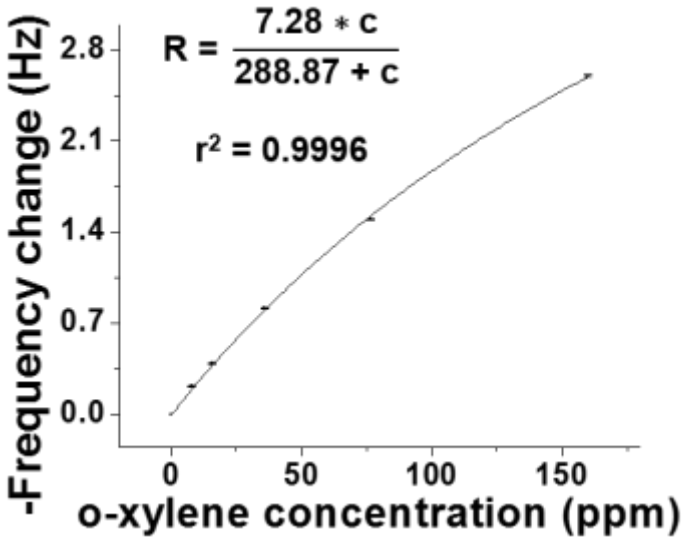

Figure 4.2 Sensor calibration under different concentrations of o-xylene.

As described in the Antoine equation [78] and chapter 3, chemical vapor pressure rises with the increase in temperature. This will induce a temperature related difference on our sensor sensitivity since higher vapor pressure can reduce adsorption of the VOC molecule on the MIP. To ensure VOC device accuracy, we calibrated the VOC device's sensor sensitivity under three different temperatures (see Figure 4.3a and previous chapter) Langmuir adsorption fitting was also applied for calibration. As discussed in our

previous chapter and publication [61], the two calibration factors, R_{max} and K_D, were defined in each fitted curve. The relationship between temperature and these two factors is presented in Figures 4.3b) and c). Results show that both KD and Rmax decreases with increment of temperature. Each batch of sensor is calibrated under these three temperatures, which is considered as a unique characteristic and will be implemented into the batch QR code. The relationship is considered to correct the VOC device's sensor response to provide accurate analyte concentration readings.

Hence we use calibration factors obtained from above (relationship between temperature with R_{max} and K_D, discussed in chapter 3), Langmuir adsorption isotherm, and sensor manufacturing information to implement a QR code for each batch of sensor to achieve a better accuracy for point-of-use detection.

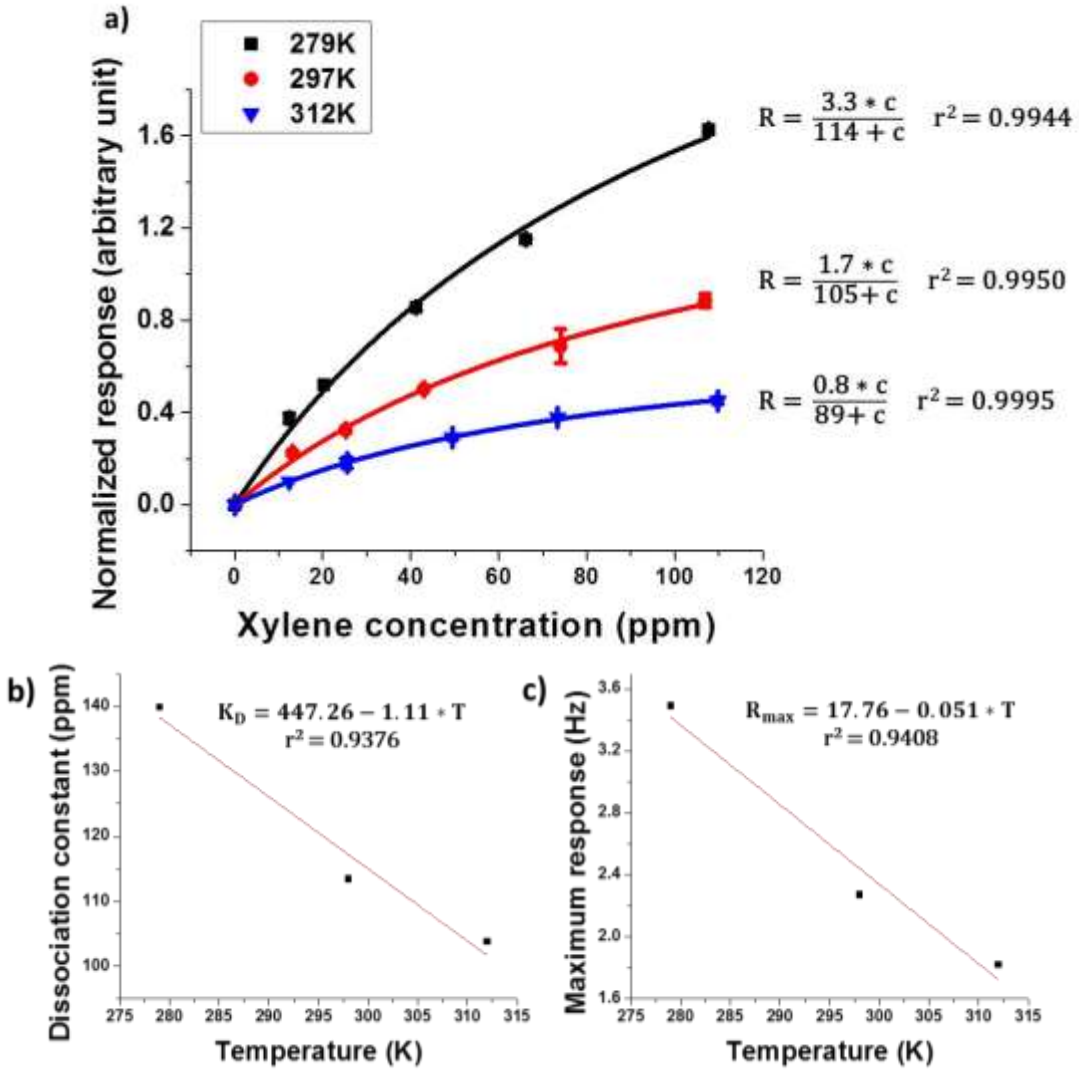

Figure 4.3 Temperature correction on sensing response a) Calibration under different temperature; b) Linear fitting of K_D to temperature (T); c) Linear fitting of R_{max} to temperature (T)

It is important to mention that due to the different hydrocarbon distribution in different environmental conditions (i.e., indoor air, outdoor air, industrial air), different calibration factors have been defined for the VOC device in order to get the final calculated total hydrocarbon concentration in ppmC. These calibration factors are based

on distributions of the different hydrocarbons, and the sensitivities of the MIP-QTF sensor to the individual hydrocarbons in the sample [31]. The hydrocarbon distributions were extracted from literature [79, 80]. The different distribution scenarios can be chosen from the user interface of the new VOC device.

Selectivity of the MIP-QTF sensors to major hydrocarbons and interferents has been shown in chapter 2. Another important feature of the new VOC device is the sensor fabrication reproducibility. MIP-QTF sensors prepared in batches of typically 200 sensors, fully assembled as replaceable sensors, and calibrated using artificial xylene sample showed a reproducibility of 9% (100% × SD/mean value).

3.3 Sensor QR Code

From what have been discussed, there are two factors intrinsically influencing on sensor response: time and temperature. As presented in chapter 1-3, the sensitivity will decay over time. As shown in chapter 3, the decay pattern has been studied for one year, during which response of two batches of sensors to 40ppm o-xylene was tested every other week or every month in the last three months (Fig. 3.3b). The patterns under different sample concentration are similar (not shown), thus we use 40ppm o-xylene as a standard gas sample in this test.

All information needed to correct the sensor response is summarized in Table 4.2. A 56 digits QR code is generated for each batch of sensor (typically with the amount of 200). In Table 4.2, T denotes temperature, t denotes time in dates and R_{40ppm} is the sensor response to 40ppm pure o-xylene. With the pre-calibrated results and QR code, it is easier

for users to get a precise monitor result without previous lab-calibration design requirement.

Table 4.2 Parameters used in QR code

Parameters	**Value**	**Comment**
Variable A	-1.11	Slope of linear fitting of K_D to T
Variable B	447.26	Intercept of linear fitting of K_D to T
Variable C	-0.051	Slope of linear fitting of R_{max} to T
Variable D	17.26	Intercept of linear fitting of R_{max} to T
Variable E	-15.66	Slope of linear fitting of R_{40ppm} to log(t)
Variable F	101.84	Intercept of linear fitting of R_{40ppm} to log(t)
Manufacture Date	07/12/2014	Date when the manufacture is done
Batch number	2014071500000 00500	Packaging date & sensors number

3.4 Personal VOCs Exposure Monitor

To identify the effectiveness of real-time personal VOCs exposure monitor, the device was used to monitor the environmental air while a user was running from home to work on Arizona State University campus. Figure 4.4a) presents the sensor QR code scanning procedure and Figure 4.4b) shows the replacement of a new sensor cartridge before the test. The user wore the device on his armband during 50 min of running. Real-time results from the new total VOC device are shown in Figure 4.4c) along with other

fitness data (such as average pace and average heart rate) simultaneously recorded in the smart phone with a mobile application (Run Keeper®, Boston, MA, USA). The real-time VOC levels from the new VOC device are plotted and shown in comparison with the running route map. As shown in the map, when the user location approaches Arizona Highway Loop 101 and other major intersections, increases in VOC levels were observed due to the heavier traffic, which introduce more VOCs to the environment atmosphere.

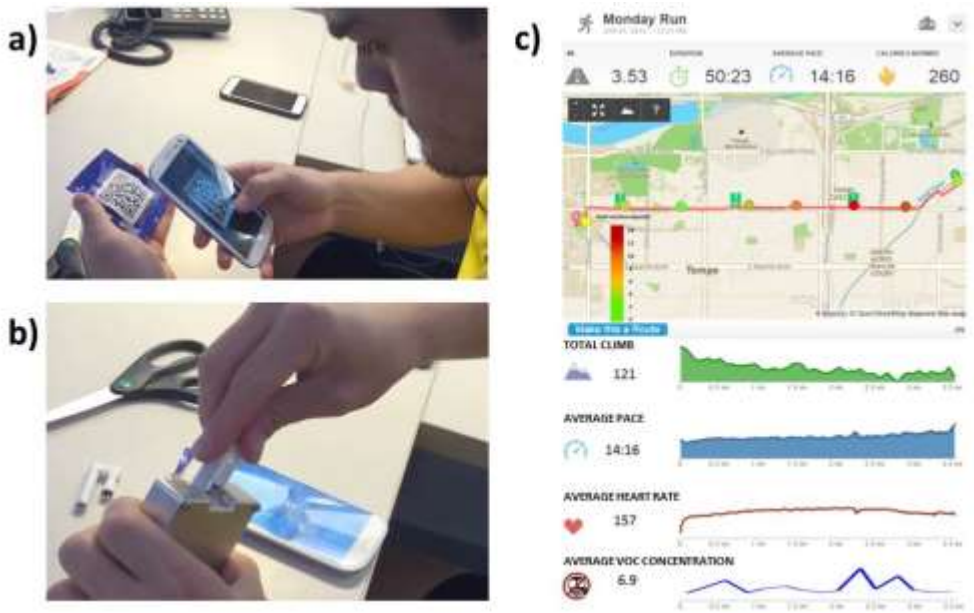

Figure 4.4 (a) Scanning sensor QR code; (b) Replacement of new sensor cartridge; (c) Real-time fitness and VOCs exposure device data during personal exercise.

This test demonstrates the ability of the device as a personal VOCs exposure monitor. With simple operation and an intuitive data presentation as shown in Figure 4.4, people can monitor their real-time VOC exposure level as simple as other fitness data.

3.5 Device Comparison with Current Technology and Commercial Device

3.5.1 Response Comparison with Photo Ionization Detector (PID)

The photo-ionization detector (PID) is a popular portable device for detecting volatile compounds by ionizing VOC molecules using a UV lamp [17]. In order to compare against current technology, a simultaneous test of the new VOC device with a PID was run with both devices placed inside a vehicle traveling along Los Angeles Highway 101 for ~40 min. The new VOC device gave a concentration value every three minutes. The PID monitor reading was also recorded at the same time. Figure 4 shows the response comparison between the new VOC device and the PID monitor. The scenario chosen to determine the total hydrocarbon concentration with the new VOC device was "outdoor environment with motor vehicle exhaust" distribution [31]. On the other hand, for the PID monitor, the correction factor for a mixture (CF_{mix}) was calculated according to the PID manual, which indicates to use the sum of the mole fractions Xi of each component divided by their PID's respective correction factors CF_i as follows:

$$CF_{mix} = 1/(X_1/CF_1 + X_2/CF_2 + X_3/CF_3 + ... X_i/CF_i) \quad 4\text{-}1$$

Due to the difference in data processing methods of the two monitors, the new VOC device gives hydrocarbon concentration in ppm Carbon (ppmC), while PID gives the concentration in ppm, rendering different final readings. However, as shown in Figure 4.5, overall average changes of readings from the two devices over time correlated well with each other (except for the first three points, where there is a potential confounding

factor during device warm-up). The raw output from VOC device and PID in this field test qualitatively show that this two methods correlates well with each other in terms of general change over time. In order to quantitatively compare the results at same scale, the readouts are converted into relative response (all data points are divided by the maximum value obtained from this test). First three data points are excluded. A paired t test is performed on data shown in Fig. 4.6. This suggests that the new VOC device has comparable real-time effectiveness to detect changes of hydrocarbons as the PID monitor under an outdoor scenario with motor vehicle exhausts.

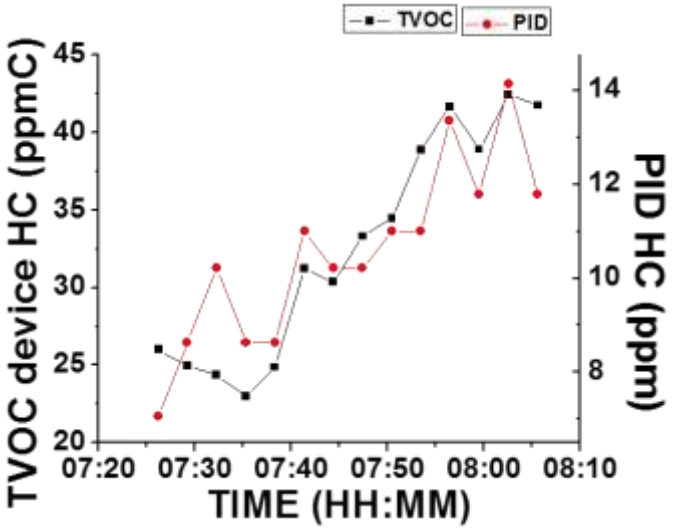

Figure 4.5 Comparison of the response between the new VOC (TVOC) device with a MIP-QTF sensor and RAE Photo-Ionization Detector (PID) for levels assessed during a trip on Los Angeles Highway 101.

NOTE: The response of TVOC was calculated in ppmC using a calibration factor for “outdoor environment with motor vehicle exhaust” (see text for more details), while

the response of PID was calculated in ppm using the calibration procedure described in the instrument manual.

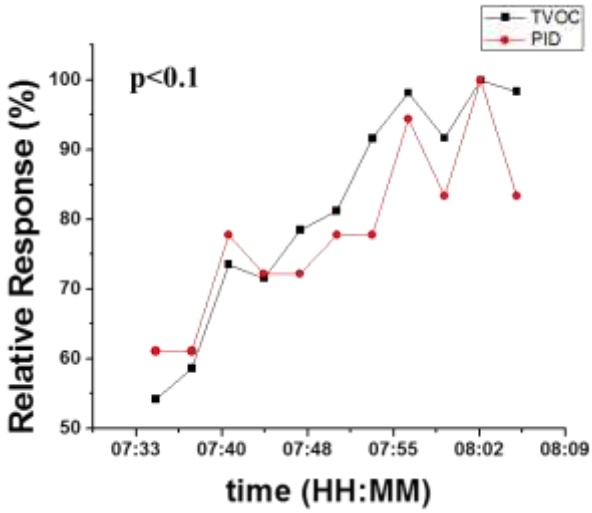

Figure 4.6 Relative response of VOC device and Photo Ionization Detector for levels assessed during a trip on Los Angeles Highway 101

3.5.2 Selectivity Validation Example with GC-MS

Due to the nature of sensing material (MIP), MIP-QTF sensors are able to detect analytes in the hydrocarbon chemical family. In order to probe the selectivity of the sensors, an environment with a dominant single gas was chosen for field-testing, and the ambient air at Mammoth Spring, Yellowstone National Park was tested. Real-time concentrations with the new VOC device were assessed while air samples were collected for GC-MS analysis in the laboratory later. Figure 4.7 summarizes the results. Artificial gas sample was tested in the lab to show that the sensor can selectively respond to hydrocarbons in the presence of H_2S. As shown in Figure 4.7, response to 6 ppm *o*-

xylene was recorded in the presence and absence of 20 ppm H_2S. There was no significant change in response with the addition of H_2S, confirming that the VOC device's sensor is immune to H_2S. Results of real-time hydrocarbon concentration from the new VOC device (Figure 4.7b) and analysis from GC-MS (Figure 4.7c,d) are compared. The hydrocarbon concentration given from the new VOC device was close to 0, indicating a low hydrocarbon concentration in the environment. However, the GC-MS analysis indicated the presence of a single strong peak of H_2S (at 1.8 min in the gas spectrum). Although a quantitative analysis was not conducted (e.g., calibration curve on GC-MS), this qualitative result provides evidence of selectivity of the VOC device with MIP-QTF sensors in highly enriched H_2S environments.

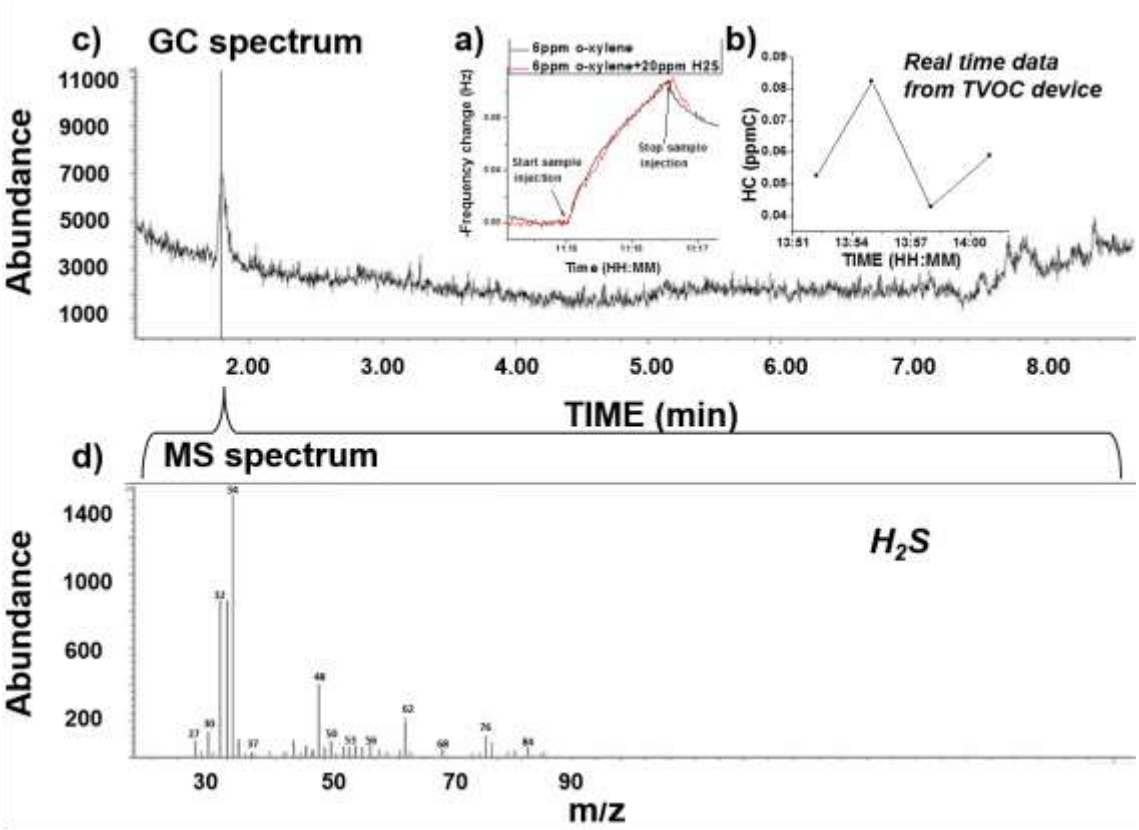

Figure 4.7 Selectivity validation test to H2S with artificial gas sample (a) and gas sample from Mammoth Spring, Yellowstone National Park. Real-time test was done on the new VOC device (b) and gas sample was collected for GC-MS analysis in the lab (c and d). The single peak in the chromatogram confirmed non-significant concentrations of other VOCs, and a presence of H2S.

3.5.3 Correlation with Carbon Monoxide Concentration

As mentioned above, a commercial carbon monoxide (CO) monitor was used to record CO concentrations while VOC concentrations were also recorded using the VOC device. The VOC device and the CO monitor were placed at the same spot, beside a local

highway in Phoenix (AZ, USA) for 12 h. During this period, both hydrocarbon and CO concentrations were recorded continuously. Due to the difference in sensing mechanism between the devices, VOC device's results were reported as an averaged concentration point every three minutes, while CO monitor gave an average concentration every minute. Figure 4.8 shows the real-time results for (a) CO concentration and (b) total hydrocarbon concentration profile, indicating that the two concentrations correlate very well, simultaneously showing: (1) A relative low level of target analytes due to light traffic from 00:00 a.m. to around 07:00 a.m.; (2) a relative larger fluctuating levels with higher concentration range from 07:00 a.m. to 12:00 p.m., coincidentally with heavier traffic. The temperature record indicated that there was no temperature inversion effect (will be discussed shortly) on the date of Figure 4.8. In addition, CO data was corrected by temperature. Furthermore, it is worthy to notice, that CO levels is expected to correlate with hydrocarbon levels, since both are incomplete combustion products of gasoline.

Same profiles could be reproduced in different days, reflecting a common profile of most daily transportation activities, which usually starts from morning and will stay busy during daytime. As mentioned in Section 3.1.2, since a big portion of HC concentration at residential comes from vehicle emission, the increase in traffic will cause a corresponding increase in HC concentration. The result demonstrated that hydrocarbon concentration from vehicle emission correlates well with real-time traffic pattern.

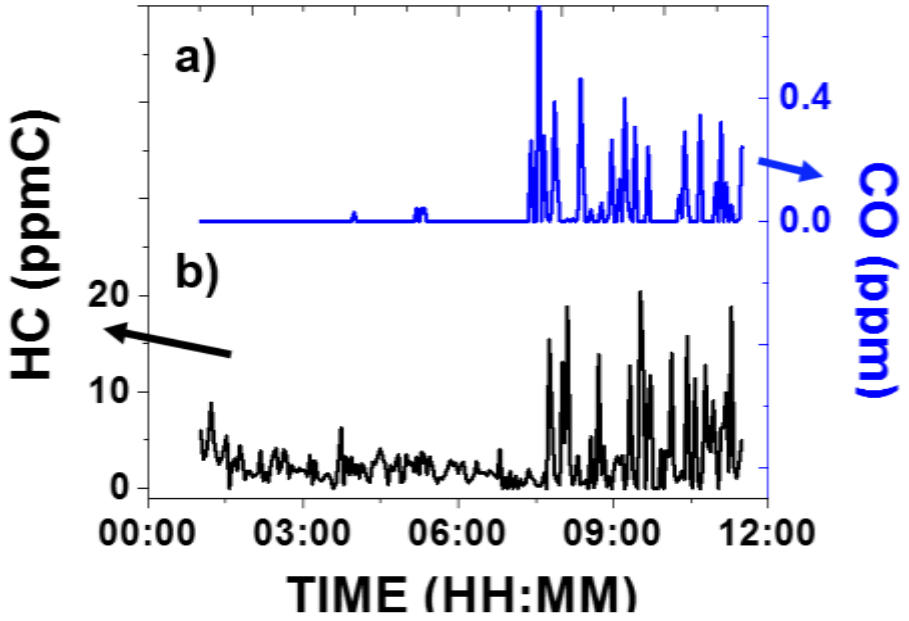

Figure 4.8 Outdoor testing of traffic markers as a function of time (a) Concentration of Carbon Monoxide, (b) Corresponding concentration of total hydrocarbon (HC).

3.6 Device Validation under Different Scenarios

3.6.1 Barometric Effect

Pressure changes due to barometric changes are potential candidates that may affect device performance since it influences the environmental operational conditions of the tuning fork sensor, which can be sensitive to pressure [81, 82]. In this field test, the VOC device was tested together with the PID monitor, while driving a car from the bottom of Trail Ridge Road, Rocky Mountain National Park (CO, USA) for 50 min, with an average speed of 35 miles per hour (MPH). This trip experienced a sharp elevation increase from 5280 ft to 12,183 ft, with an associated pressure drop of ~35 kPa from the

beginning to the end [83]. As shown in Figure 4.9, both the new VOC device and PID monitor readings were recorded. It can be observed that the two devices were not affected by the barometric change in an obvious way, and the results were comparable with each other. This fact also demonstrated that the new VOC device can perform stably under sharp barometric changes. It is worth noticing that the immunity of the VOC device to pressure is attributed to the sample collection and delivery mode with a switching valve between purging and sampling channels, enabling baseline corrections right before each sensing period (as explained in the experimental section).

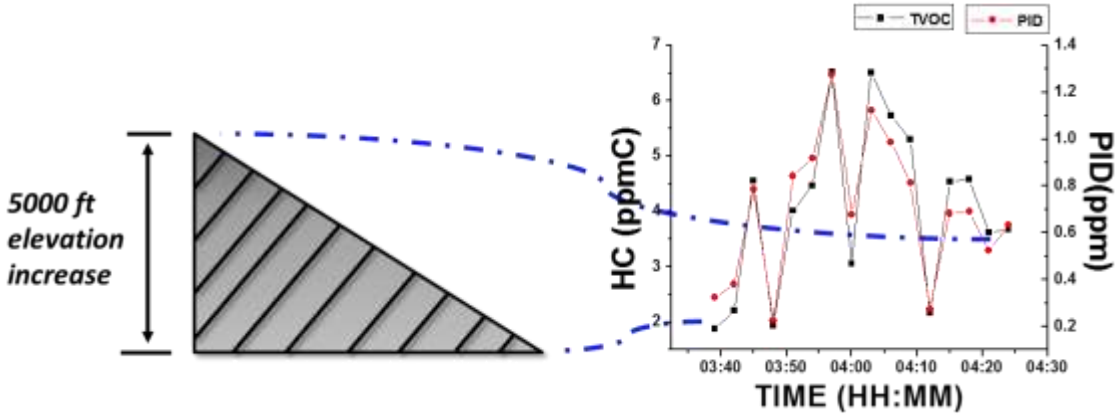

Figure 4.9 The new VOC device's performance to a rapid elevation increase. Starting point and end point of the trip are indicated using dashed-dotted lines.

3.6.2 Temperature Inversion Effect

A test was conducted to inspect the effect of ambient temperature change to the VOC device performance. As shown in the picture in Figure 4.11, the device (indicated as point A in the picture) was physically located on the roof of an environmental station. Hydrocarbon concentration was monitored for 12 h continuously together with the

temperature from sensors located at points A and B. Figure 4.11 shows the HC concentration profile (a) in connection with the temperature profile (b) recorded for 12 h. From 00:00 a.m. to 07:00 a.m., the hydrocarbon level remained at a low level, reflecting a relative steady and low hydrocarbon concentration scenario. Starting from 07:00 a.m., HC concentration fluctuation increased, at which time, a change in temperature pattern was also noted (see below).

Figure 4.10b shows the temperature difference between point A (roof temperature) and point B (ground temperature) vs. time. A change of the temperature difference from positive to negative at ~7:00 a.m., known as inversion temperature, is shown in Figure 4.11b, and an obvious drop of HC concentration in the profile at the same time (~7:00 a.m.) is shown in Figure 4.11a. When the difference between roof temperature and ground temperature is changing from positive to negative, a well-known natural convection phenomenon occurs [84], leading to a dilution of pollutants in the air. This is expected to reduce the concentration of hydrocarbon, and was reflected as a transitory decay of HC concentration reading from the VOC device. This result shows the effectiveness of the VOC device to capture real-time HC concentrations due to environmental changing conditions such as temperature.

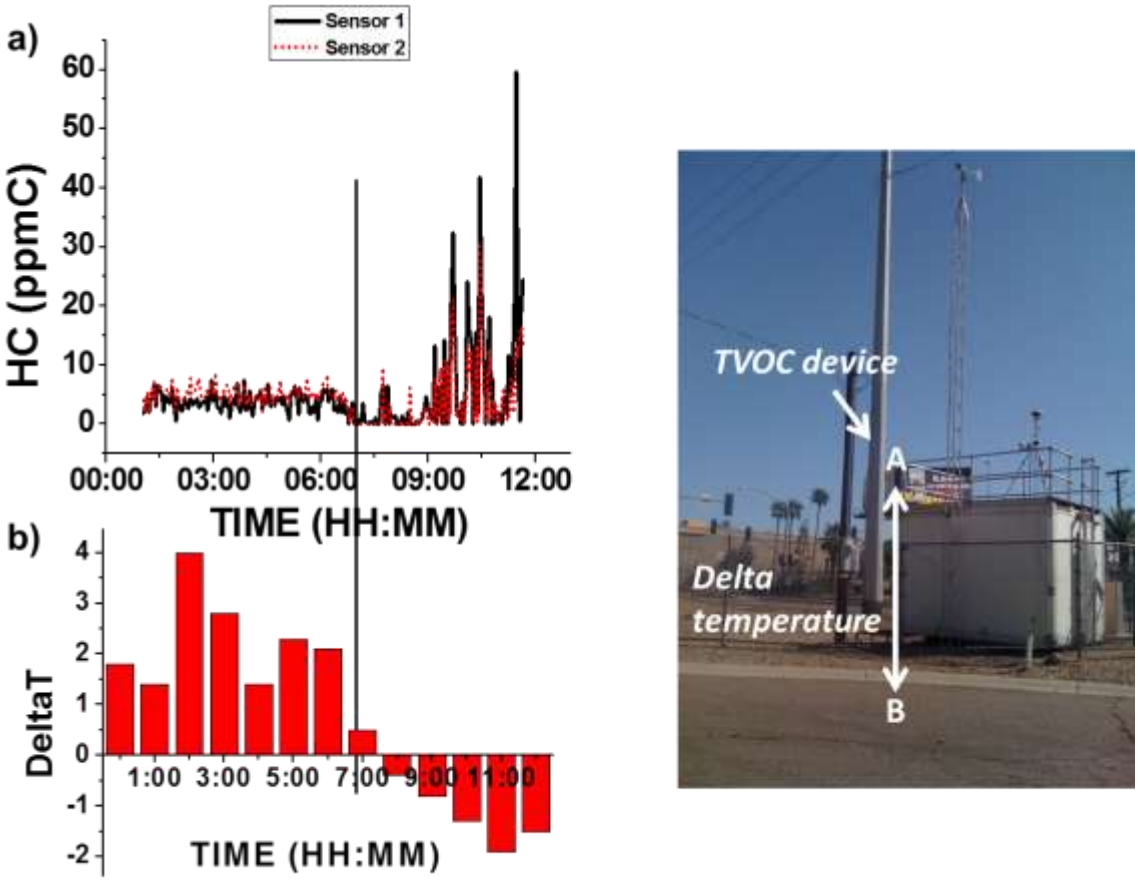

Figure 4.10 Temperature inversion effect (a) VOC device's real-time hydrocarbon concentration test at point A. (b) Corresponding delta temperature between points A and B. Height between point A and B was 14 ft.

3.6.3 Wind Condition Effect

Wind condition will cause gas movement and redistribution of atmospheric components. To study the wind effect, we chose an environmental station from Maricopa Air Quality Department at the intersection of Arizona highways I-10 and I-17. The VOC device was placed at the same spot for two business days, for 12 h each day, detecting the

hydrocarbon (HC) concentration profile. Wind speed and direction were recorded simultaneously. The data obtained from two testing days are presented in Figure 4.12 a,b. Average wind speed on Day 1 was (1.1 $\pm$0.9) MPH and direction was from the east side of the testing location, which is marked as Direction A in Figure 4.12 d. Average wind speed on Day 2 was (3.6 $\pm$2.5) MPH. Direction B in Figure 4.12d indicates the wind direction on Day 2. Direction A was from Arizona I-17 Highway and through a local truck center, which might potentially bring VOCs towards the testing location. Direction B was from a local residential area, which usually has low VOCs concentration.

Similar to the cases described in Sections 3.2.4 and 3.3.1, both Figure 4.12 a,b shows a relatively low HC concentration from 00:00 a.m. to 07:00 a.m. due to the light traffic and low activity level. However, a significant difference is observed in the time window from 07:00 a.m. to 10:00 a.m., with the case shown in Figure 9a having a much higher level of HC concentration than the case shown in Figure 4.12 b. Since the two testing days were normal business days, traffic conditions on each day were expected to be similar. However, the HC concentration profiles (Figure 4.11 a,b) and peak HC concentration values (Figure 4.11 c) on the two days were significantly different. This result suggests that higher HC concentration levels were associated with lower wind speed and wind direction from areas with higher traffic such as a local truck center and highway. Likewise, higher wind speed and wind direction from cleaner locations had a lower expected HC concentration.

It is worthy to mention that in our sensor cartridge design, the small size of the sensor allows the assembly of the two identical sensors (sensors 1 and 2) inside the same

sensor cartridge. The similar profiles (shown in Figure 4.11 a,b) by the two sensors suggested reproducible environmental hydrocarbon detection capability of the VOC device. In addition, the dynamic response of the sensors in real-time remains constant throughout the lifetime of the sensors is shown in Figure 4.12.

Although the above-mentioned combined effect of wind speed and wind direction to HC concentration is predictable, it is worth noticing the new VOC device responded in an expected way when it was interrogated under higher windy and cleaner air source conditions. This analysis future confirms the validity of the VOC device even in uncertain wind conditions.

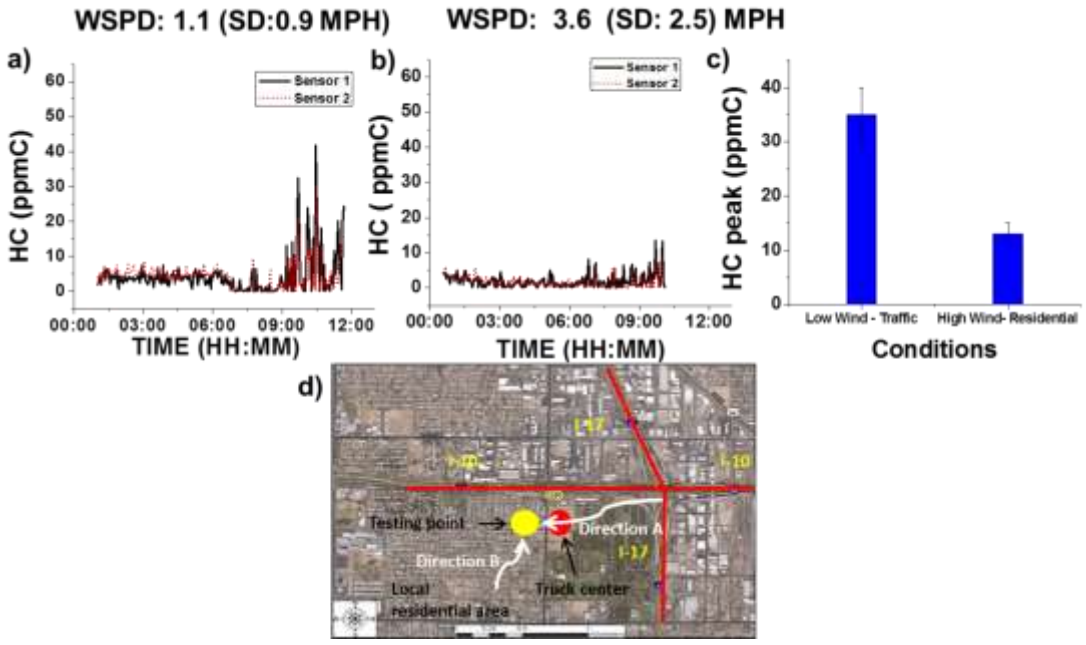

Figure 4.11 Wind speed and direction effect on VOC device performance (a) HC concentration under lower wind speed and wind direction from areas with higher expected concentration (direction A showing in (d), (b) HC concentration under higher wind speed and wind direction from areas with lower expected concentration (direction B showing in (d); (c) peak HC values comparison; (d) a map showing the testing location and wind directions.

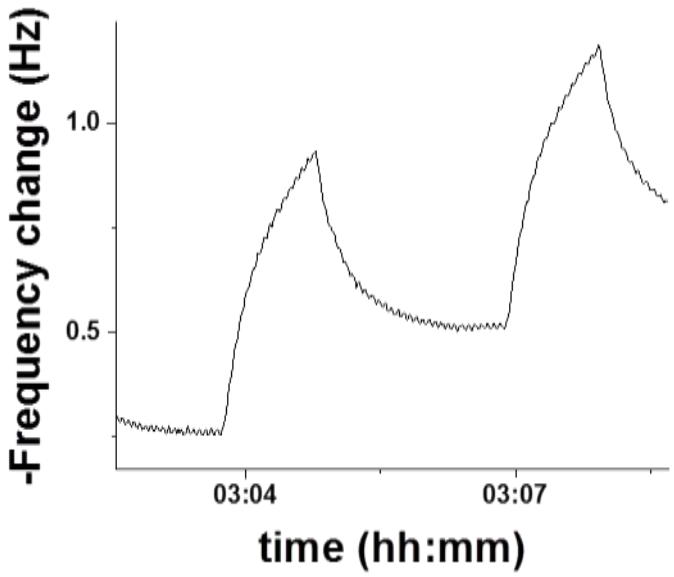

Figure 4.12 Real-time response of VOC device to 40 ppm xylene on a modified tuning fork sensor. The baseline of the new injection is taken from the purging time slope assessed in the previous injection. Since the MIP has high surface to volume ratio the number of binding sites are sufficient to conduct the measurements of the hydrocarbons during the lifetime of the sensors, which was defined to be 464 ppmC ћ.

4. Conclusions

In this chapter, the new portable wireless QTF sensor-based VOC-sensing device system is presented. Comparison of the VOC device to its previous version indicates that improvements to make the device smaller, lighter, and more user-friendly have been accomplished. The device has demonstrated adequacy as a personal VOC exposure monitor. The different field tests to evaluate the analytical, functional and usability performances of the new VOC device and its sensor have been satisfactory. Results

showed good correlations between: (1) The VOC device and commercial PID monitor in outdoor air with motor vehicle exhausts, (2) the VOC device and GC-MS to reassure negative detection of gas in an environment enriched with single gas of H_2S, (3) good tolerance of the VOC device response to a barometric change, and (4) real-time correlation with CO. The VOC device also showed fast response towards changes in ambient environmental operational conditions such as wind and temperature inversion. In conclusion, this upgraded portable VOC device together with the pre-calibrated sensor cartridge and new user interface (application) can be used in different real-world scenarios and is applicable to personal daily use.

CHAPTER 5

Exploration on relationship between VOCs exposure with resting energy expenditure

ABSTRACT

Obesity, an epidemic with associated conditions increased in all age groups for the past three decades. RMR, also known as resting energy expenditure (REE) is the basic metabolic rate at resting state. It represents the minimum energy needed to sustain life. It is one of the key factors for weight management. There has been research reported that the persistent organic pollutants (POP) may decrease skeletal muscle oxidative enzyme, inhibit mitochondrial activity and decreased thyroid hormone levels. To explore more on how these organic pollutants are impacting on metabolism, a study was conducted. In a single blind, acute, placebo-controlled, crossover open label study and after an initial familiarization visit, 40subjects (male: n = 23; female: n = 17; Age: 28.2 ±5.3 y; body mass index = 23.1 ±3.8 Kg/m^2; Body fat (Bio-impedence): 18.6 ±7.2%) underwent testing sessions with metabolic tracker breezing equipment during which time they consumed either a 2 mg capsaicinoids supplement (100 mg Capsimax®) or placebo, one capsule/d. At least 35 subjects are required to satisfy a power of 0.95 with an α of 0.05. Hydrocarbon concentration in 10 common scenarios was tested using the hydrocarbon device. Results show that there is a significant REE increment from the supplement treated group comparing to control group. For VOCs exposure, no obvious correlation was found between the exposure environment and subjects' REE.

1. Introduction

Obesity, an epidemic with associated conditions increased in all age groups for the past three decades. There is no evidence of a decline in overweight and obesity prevalence in any age group for the past 10 years. Obesity may cause heart disease, type II diabetes, and etc. [85]. This epidemic is influenced by many factors such as gene, living environment, and diet habit [86]. The prevalence of obesity is increasing globally [87, 88].The increased rate of obesity in the past decade is caused by a larger rate of energy intake than expenditure [89].

RMR, also known as resting energy expenditure (REE) is the basic metabolic rate at resting state. It represents the minimum energy needed to sustain life [90]. It is one of the key factors for weight management. Technologies have been developed to measure REE. However, traditional indirect calorimetry device is bulky and expensive, making it unrealistic and inconvenient for people to track their REE at real-time. To fulfill the needs, a mobile indirect calorimeter, Breezing® was developed to facilitate personalized REE measurement. Based on optical detection of chemical sensor cartridge [91], oxygen consumption rate (VO_2) and carbon dioxide production rate (VCO_2) in breath is determined. According to the Weir equation [92], REE is determined by VO_2, VCO_2 and breath flow rate, which is measured by a commercial flow sensor implemented inside the device.

The Breezing® device evaluates people's energy expenditure (EE) by detecting the rate of oxygen consumption and carbon dioxide generation in breath. It is based on a

flow meter for flow detection and a chemical sensing cartridge, which used a cell-phone camera for optical detection. As reported before [90], Fig. 5.1 shows the testing configuration of the current Breezing® device. The device is 6.0 oz. (170 g), and 1.8 in × 2.1 in × 4.8 in (4.7 cm × 5.4 cm × 12.3 cm), and connects wirelessly to an iOS/Android mobile device, via Bluetooth®. A QR code with pre-calibrated sensor information is applied on the single-use sensor cartridge, which can be scanned and recognized by the mobile application.

During each measurement, participants breathed through a disposable mouthpiece connected to the Breezing® device for about 1-2 minutes until a total of 6L exhaled breath were measured by the flow meter.

The data received on the mobile device is processed and displayed on the application. According to Weir equation, RQ, VO_2 and VCO_2, the energy expenditure is determined.

Epidemiological models about correlation between REE and physical parameters have been reported in the past decades [93-95]. These equations show the average REE level. However, individual REE level may vary a lot from the average value.

There has been research reported that the persistent organic pollutants (POPs) may decrease skeletal muscle oxidative enzyme, inhibit mitochondrial activity and decreased thyroid hormone levels [96, 97]. With lower metabolic activity, lower resting metabolic rates (RMR) has been found. Lower RMR is directly associated to gain weight, or difficulty to lose weight in people undergoing weight loss plans. This brings the

obesity problem up from as issue of environmental health. There are a lot of possible factors that may potentially induce the different REE level on people with similar physiology condition. For example, whether the exposure to POPs is also influencing on the REE has never been reported.

In the past few years, a lot of work about weight management and fat loss has been reported. One of the possible aids with scientific support is capsaicinoids. Capsaicinoids, 8-methyl-N-vanillyl-6-nonenamide, is found in chili peppers and their extracts. It has been reported to increase thermogenesis [98-100] and decrease chances of obesity [101].

Figure 5.1 Breezing® device The Breezing® indirect calorimeter, sensor cartridge, mouthpiece, and iPhone interface of the application[90].

2. Materials and Methods

Two parts of experiment have been designed:

1. REE level enhancement with a Capsaicinoids supplement;
2. REE level and its variance correlation with POP exposure.

The part 1 is planned to study the impact of a Capsaicinoids supplement on people's REE level. This is to learn about weight management in terms of diet intake.

In order to study the above stated issue, we use the Breezing® device to track participants' REE change. 40 volunteers were hired and 80 tests were done. Both REE change and heart rate profile were recorded. Statistical analysis methods, such as power calculation statement and paired t test, would be used to evaluate the results. In the meantime, subjects' REE level will be divided into groups and their daily living/working environment will be monitored.

Information of participants has been summarized in Table 5.1. And individual participant's information has been recorded in Table 5.2.

Table 5.1 Summary of participants

		Age (yr)	Height(in)	Weight(lbs)	BMI(lbs/in^2)	Bioimpedance(%)
Male	23	28.3±5.5 (22-47)	66.6±4.7 (61-75)	146.8±32.8 (116-209)	23.1±3.9 (18.1-31.8)	18.0±7.2 (6.0-26.7)
Female	17	28.1±5.4 (23-47)	66.4±4.7 (56-69)	145.4±32.5 (99-185)	23.0±3.8 (17.2-32.8)	18.4±7.2 (13.2-44.4)
Total	40	28.2±5.3 (22-47)	66.4±4.7 (56-75)	145.7±32.8 (99-209)	23.1±3.8 (18.1-32.8)	18.6±7.2 (6.0-44.4)

Table 5.2 Information of every participant

Subject #	Gender	Age/yr	Height/in	Weight/lbs	BMI/kg m^2	Bioimpedance(%)
1	F	26	64	131	22.5	26.3
2	M	31	69	143	21.1	9.5
3	M	31	70	158	22.7	15.1
4	M	24	72	159	21.6	12.3
5	M	28	71	130	19.2	6
6	F	23	56	102	21.3	13.2
7	F	23	66	137	22.1	25.9
8	M	22	69	207	30.6	26.6
9	M	27	68	175	26.6	17.3
10	F	47	63	185	32.8	44.4
11	M	30	70	182	26.1	16.2
12	M	31	65	175	29.1	22.2
13	M	28	69	163	24.1	17.7
14	M	26	75	189	23.6	13.6
15	M	31	67	116	18.2	6.3
16	M	26	71	146	20.4	11.4
17	M	36	72	177	24	16.6
18	M	34	67	134	21.0	12.2
19	M	27	68	209	31.8	26.7
20	M	24	73	181	23.9	17.2
21	F	26	63	127	22.5	22.8
22	F	24	56	101	22.6	16.3
23	M	27	69	142	21.0	11.3
24	F	29	59	99	29.0	19.4
25	F	25	64	100	17.2	14.2
26	F	25	63	104	18.4	14.8
27	F	24	60	116	22.7	22.5
228	F	29	62	109	19.4	22.1
29	F	26	62	111	20.3	18
30	M	27	61	176	23.2	18.8
31	F	30	61	116	21.9	29.2
32	M	23	70	178	25.5	25.7
33	M	28	70	174	25.0	15.9
34	F	26	67	130	20.4	24
35	F	26	63	104	18.4	15.6
36	M	30	70	126	18.1	8.3
37	M	25	70	172	24.7	16.2
38	M	47	72	178	24.1	19.6
39	F	23	69	153	22.6	28.2
40	F	27	61	101	19.1	16.9

2.1 Capsaicinoids Extract Supplement, Capsimax®, Omnihealth Technology

Capsaicin, the compound that gives red chili pepper its powerful kick, creates the largest bump in heat generation, which helps burn more calories immediately after a meal. It helps in healthy weight management. The supplement used in this study contained 2 mg capsaicinoids per 100mg capsule. And the placebo capsule consisted of microcrystalline cellulose.

2.2 Effect of Capsicum Extract Supplement on People's REE

Before each test, the participant arrived without any food intake in the past 4 hours, and no strenuous exercise performed for 12 hours before the test, or no moderate exercise performed at least 4hours before the test. Once the resting state was assured, their REE would be measured. At least 2 consecutive measurements of REE were taken to assure accuracy. In addition, participants' weight, height, and fat% were assessed with Tanita bio-impedance scale, and a wall ruler. After that, participants were instructed to wear a Zephyr chest strap tracker for physiological parameters' monitoring.

The participants were provided with meal including a non-caloric, decaf drink and certain amount of Thomas Plain Bagel and 1/3 less fat Philadelphia cream cheese based on their REE level. The ratio of calorie intake to their REE value was 0.35 for 14 participants and 0.25 for 25 participants. In the meantime, the participants were served with either a Capsaicinoids pill or a placebo pill. The placebo will pair the supplement size and physical characteristics. Each participant took the test twice: one was served

with Capsaicinoids pill and the other one was served with placebo pill (no sequence on assigning the pill). The study was single blind. In between two tests, there was a two days wash-out period at least.

After finishing the meal/pill or the pill, the participants' metabolic rate were measured at 1 h, 2 h, and 3 h after the meal.

One complete test took around 3.5 h. During the blank time of the test, participants were required to perform sedentary office or bench work.

The testing protocol is summarized in Fig. 5.2 a).

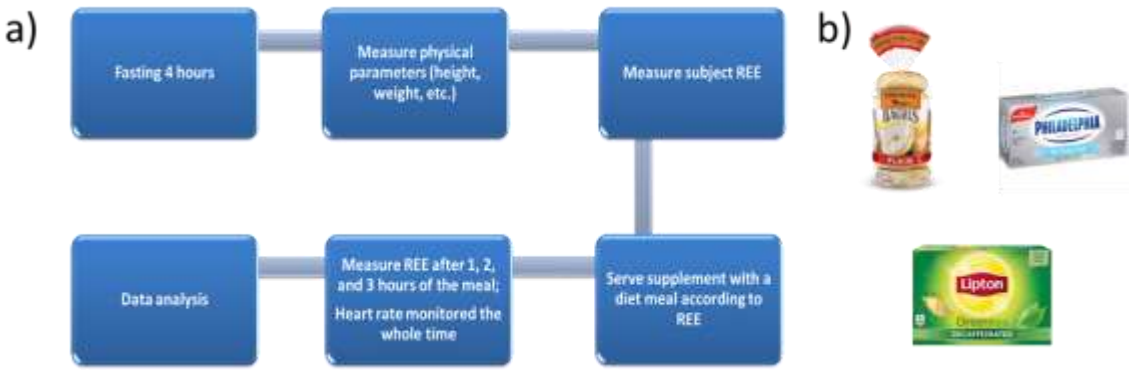

Figure 5.2 a) Testing protocol; b) Meal provided to participants

After this test, participants' initial REE would be analyzed and grouped.

2.3 Validation of REE Level and Its Variance Correlation with POPs Exposure

After the participants' REE baselines were measured, hydrocarbon concentration from daily living or working places of 17 participants was tested. Each location was

tested three times and the concentration result was averaged. As a reference, PID was also used.

3. Results and Discussion

3.1 REE Measurement

The average REE in Capsaicinoids group and placebo group of all participants are compared in Fig. 5.3. Fig. 5.3a) is the average raw REE value of all participants. Based on the same set of data, Fig. 5.3b) and c) are plotted to compare the difference between two groups at same level. The REE value before the meal was considered as baseline of that participant. REE_0 denotes the baseline REE value and REE_i represents the REE value measured at 1h, 2h and 3h. By subtracting the baseline value, relative REE change in 1h, 2h and 3h are shown in Fig. 5.3b). Fig. 5.3c) is presenting the data in terms of percentage. The data is calculated as: $[(REE_i - REE_0)/REE_0]*100\%$.

On average, the group took this Capsaicinoids capsule showed a positive REE change comparing to the placebo group. The REE level of Capsaicinoids group increased 116 Kcal/day (8%) at the end of three hours, while the placebo group shows ±15 Kcal/day (less than 0.7%) fluctuation over the whole test. This demonstrates that the Capsaicinoid pill could enhance people's REE on average.

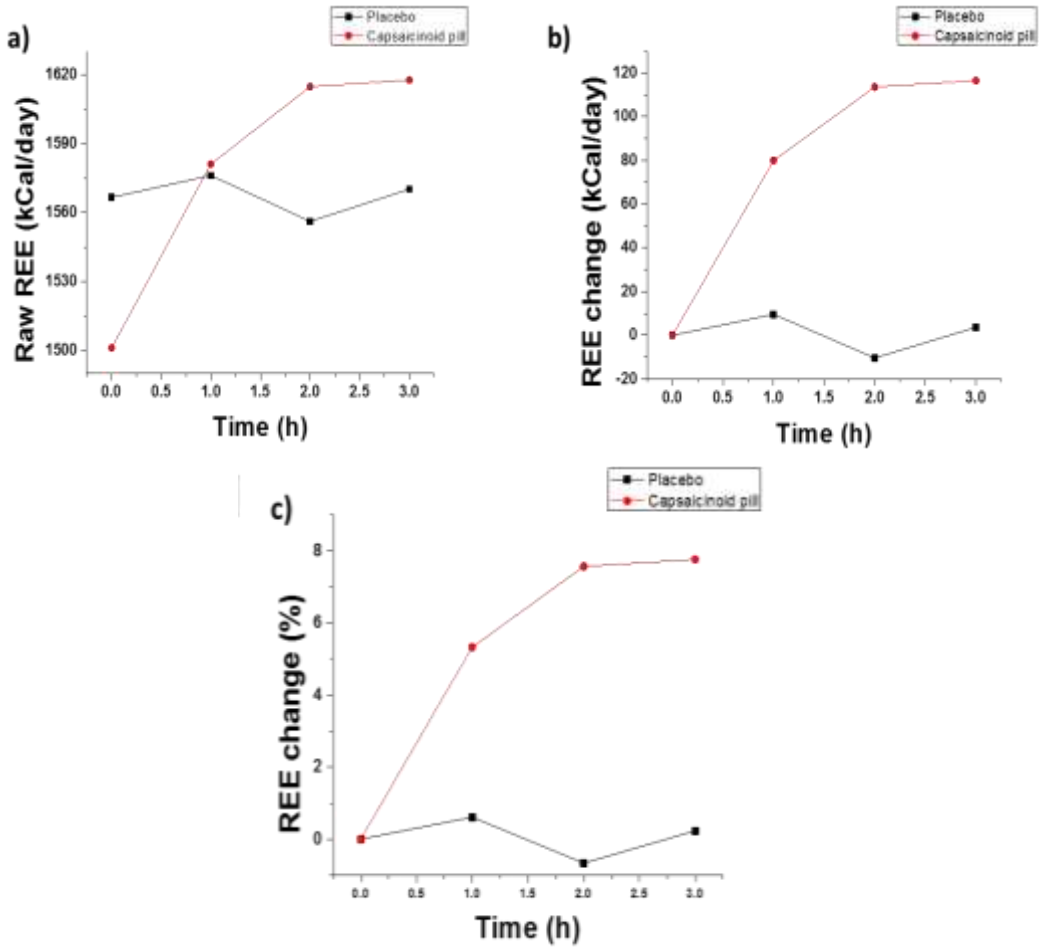

Figure 5.3 Averagea) Average REE of all participants; b) Relative average REE change (REEi-REE0); c) Relative average REE change in percentage ([(REEi – REE0)/REE0] *100%). See text for details.

Metabolic rate is unique on each individual. Fig. 5.4 shows the ΔREE% of each participant. ΔREE% of every hour after the meal and the average of all three hours data are shown. In Fig. 5.4, the label outside the radar plot indicates the participants' number. The radius label denotes ΔREE%. Participants underlined blue were served with diet 1 in

which the amount of calorie intake was 0.35 portion of their REE value. The rest of the 26 participants underlined yellow were served with diet 2 in which the amount of calorie intake was deducted to 0.25 portion of their REE value. The reason for the adjustment in diet was that participants reported that the amount of food was more than what they usually took. Thermogenesis effect from too much food intake may potentially mask the effect of the pill.

Visually looking at the graphs of Fig. 5.4, the Capsaicinoids group is at outer cycle comparing to the placebo group, meaning that the Capsaicinoids pill has a positive effect on people's metabolic rate in general. To quantitatively analyze this, absolute area integration results are shown in Table 5.3.

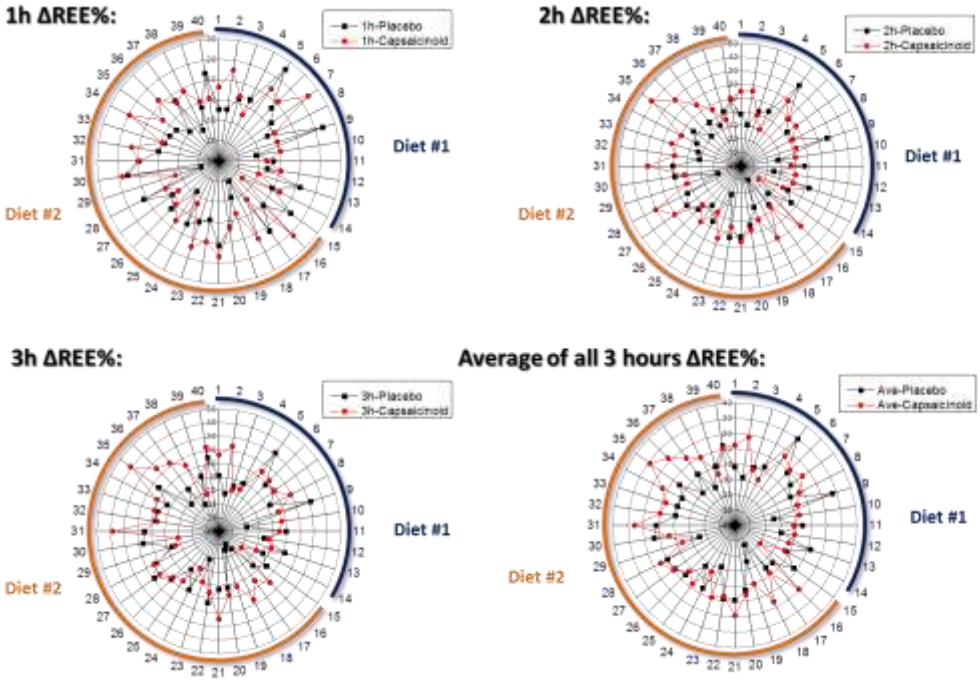

Figure 5.4 ΔREE% at different time of the test and average.

Table 5.3 Integrated areas from radar plot

ΔREE %	Group	Radar plot area integration (%)
1h	Placebo	-55
	Capsaicinoids	450
2h	Placebo	-260
	Capsaicinoids	836
3h	Placebo	-321
	Capsaicinoids	865
Average of all ΔREE %	Placebo	-212
	Capsaicinoids	717

Table 5.3 demonstrates that Capsaicinoids group has a significantly positive integrated area comparing to placebo group during the 3 hours. From the first hour to third hour of the test, the difference between Capsaicinoids and placebo group keeps increasing (from 505% to 1186%), indicating that the capsaicinoids pill induces a faster growth in REE than placebo group.

3.2 Heart Rate Profile

Participants' heart rate was monitored via a rea-time monitoring tracker, Zephyr, in the shape of a chest band (Fig. 5.5 a). Their physiology activity signal were recorded and reported to a PC interface every second. Fig. 5b) shows the average heart rate profile of all participants. The average heart rate of Capsaicinoids group is (78.6±2.72) BPM while placebo group has an average of (79.15±2.88) BPM. During the test, both groups average heart rate increased around 10 BPM in the first 30 minutes, and then gradually

recovered back to their initial heart rate. The level-up of heart rate in the beginning is due to the food injection. Fig. 5.5b) demonstrates that there is no significant difference in heart rate between two groups.

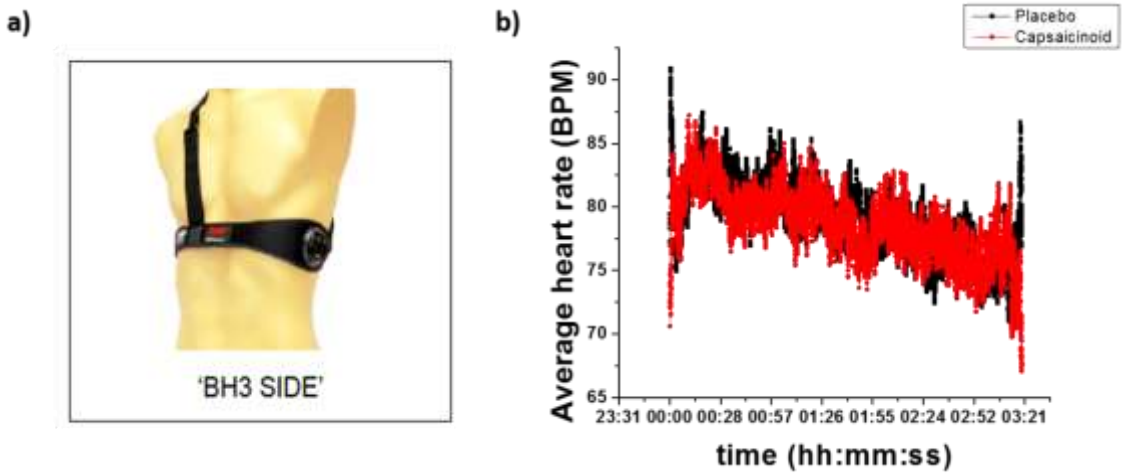

Figure 5.5 Heart rate profiles. a) Zephyr real-time activity monitor; b) Average heart rate of all participants

3.3 Statistical Data Analyzation

With data shown above, this part statistically analyzes the data to define the sufficiency of collected data and conclude with paired t-test results. Analysis and calculations are from references [102].

3.3.1 Power Calculation Statement

Fig. 5.3b) showed that the smallest average ΔREE% difference between the two groups happened at the first hour (75 Kcal/day). To satisfy a power of 0.95 to distinguish the two groups, at least 35 sample sizes is required. Thus the sample size of 40 is sufficient to conclude the difference.

3.3.2 T-test Analysis

I. Capsaicinoids VS Placebo

A paired t-test was run on the ΔREE% results shown in Fig. 5.4. In this test, α=0.05 and the degree of freedom is 39. Results are shown in Table5. 4. Table 5.4 shows that ΔREE% at 2 hour and 3 hour has significant difference between Capsaicinoids and placebo group since both of their p value are smaller than 0.05. And the average ΔREE% of all three hours also has significant difference between two groups. The p value of ΔREE% at 1 hour is 0.115. This is considered as no significant difference. Again, due to the thermogenesis effect from food, the impact of the Capsaicinoids pill might be covered at beginning.

Table 5.4 Paired t-test between Capsaicinoids and Placebo group

ΔREE %	**1h**	**2h**	**3h**	**Average**
p value	0.115	0.006	0.023	0.012
Significance	No	Yes	Yes	Yes

II. Female VS Male Participants

A t-test was run on results between female and male participants. In this test, α=0.05 and the degree of freedom is 38. As presented in Table 5.5, p value is always higher than 0.1, which is considered as no significant difference between the two groups.

Table 5.5 T-test between female and male group

ΔREE %	**1h**	**2h**	**3h**	**Average**
p value	0.48	0.62	0.72	0.78
Significance	No	No	No	No

3.4 Pre-rated REE Change

To specifically evaluate this Capsaicinoids pill, we pre-rate the REE change in 24 hours after the intake of the pill. The average REE value of all participants' baseline REE, 1534 Kcal/day, is picked for this calculation.

REE represents the basic energy expenditure in a day. Data from Fig. 5.3 c) is used to pre-rate the REE change. Table 5.6 summarizes this pre-rate example. Comparing to placebo group, Capsaicinoids group would increase people's REE more than 100 Kcal/day (6%) on average.

Table 5.6 Pre-rated REE change

Pre-rated REE changes in 24hrs / Group	**1h**	**2h**	**3h**	**Average**
Placebo	26 kCal/day (1.27%)	18 kCal/day (0.52%)	19 kCal/day (1.72%)	8 kCal/day (1.17%)
Capsaicinoids	73 kCal/day (4.79%)	130 kCal/day (8.48%)	129 kCal/day (8.43%)	111 kCal/day (7.23%)

*Pre-rated REE change= 1534 Kcal.day * ΔREE%, ΔREE% is from Fig. 5.3c).

3.5 REE Variance between Epidemiological Equations And Real Measurements

Epidemiological models about correlation between REE and physical parameters have been reported in the past decades [93-95]. These equations show the average REE level. However, individual REE level may vary a lot from the average value. Fig. 5.6 shows the tested REE difference with REE from a well-known Mifflin-St Jeor Equation based on the physical parameters. This graph shows that only 35% of participants' REE has a difference with Mifflin-St Jeor Equation within ±200 kCal/day. This indicates the importance of monitoring personal REE level, instead of getting your REE value on average.

Thus we divide the participants into 3 groups which their REE difference (ΔREE) from Breezing® device and Mifflin-St Jeor equation is A) higher than 200 kCal/day (16 subjects), 2) within ±200 kCal/day (14 subjects) and 3) lower than -200 kCal/day (10 subjects). 20 participants' daily living and working environment were measured and analyzed to study the correlation between the daily real time POP exposure and individual REE.

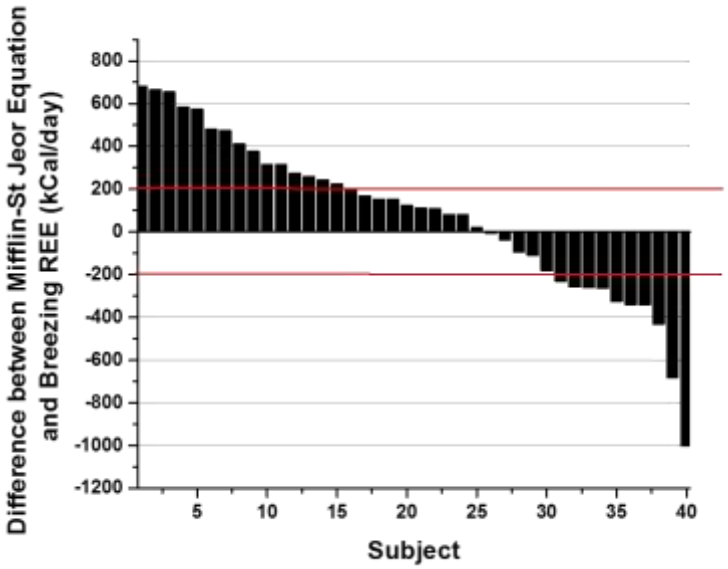

Figure 5.6 Differences between Mifflin-St Jeor Equation and Breezing REE.

Mifflin-St Jeor Equation is expressed as [94]:

Female REE (kCal/day): 655+ (4.35*weight in pounds) + (4.7*height in inches) – 4.7*age in years)

Male REE (kCal/day): 66+ (6.23*weight in pounds) + (12.7*height in inches) – 6.8*age in years)

3.6 Relationship Between ΔREE And Hydrocarbons Exposure

As talked above, 17 subjects' daily working or living environment was tested, in which 6 subjects from group A, 6 subjects from group B, and 5 subjects from group C. The locations include: laboratory spaces, office area and home. Since some subjects share the same working space, they also share the same hydrocarbon exposure environment. In

these subjects, 6 are male and 11 are female. The results are compared in Fig. 5.7 and Table 5.7. Based on subjects' activity time at office and home, the 24 hour average hydrocarbon exposure is calculated with time weight of 10 hours at daily activity area and 14 hours at night activity area.

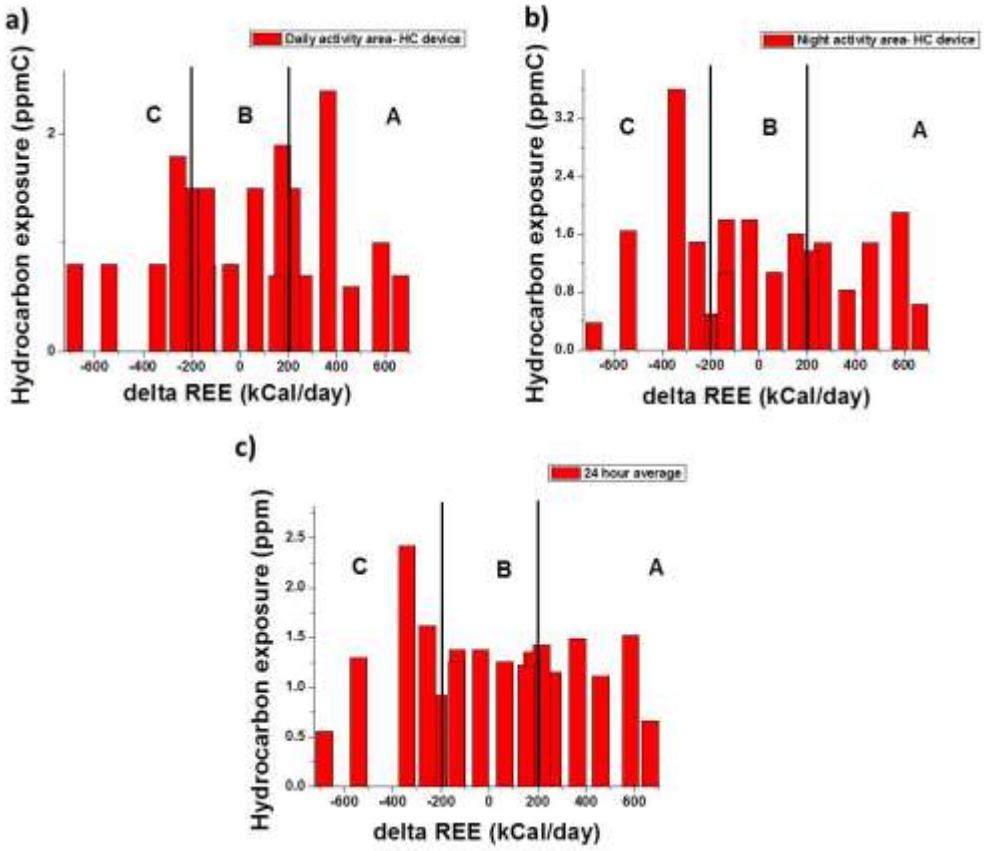

Figure 5.7 Hydrocarbon concentration at different locations exposing to 17 subjects a) Daily working activity areas; b) Night home area; c) Average exposure in 24 hours

Table 5.7 Summary of hydrocarbons exposure level at different locations

Group	A	B	C
Daily activity area HC exposure (ppmC)	1.15±0.63	1.20±0.45	1.14±0.43
Night activity area HC exposure (ppmC)	2.56±0.48	2.77±0.24	3.05±1.30
24 hour average HC exposure (ppmC)	1.97±0.48	2.11±0.24	2.25±1.30

From above results, it can be concluded that there is no significant different in total hydrocarbon concentration exposure for all groups. Although for group C, the average night activity area hydrocarbon exposure is relatively higher than the other two groups (9% to 16%), the variance from these samples is too big to define a difference.

4. Conclusion

In this chapter, a single blind, acute, placebo-controlled, crossover open label study and after an initial familiarization visit, 40subjects underwent testing sessions with metabolic tracker breezing equipment during which time they consumed either a 2 mg capsaicinoids supplement (100 mg Capsimax®) or placebo, one capsule/d. Results shown

above have demonstrated that this Capsaicinoids diet supplement could enhance REE level. And there is no significant evidence showing that there is correlation between hydrocarbon exposure and difference of epidemiology equation and Breezing device.

CHAPTER 6

Conclusion and Future Work

We have developed a wearable QTF based device for real-time hydrocarbon exposure monitor. This analyzer provides timely and accurate response of hydrocarbon level. The sensor performance depends on adsorption reaction and mass transport between gas sample and the sensing polymer. The polymer is a molecularly imprinted polymer that can selectively adsorb target analytes.

The material, sensor and device performance has been characterized in terms of sensitivity, stability, reproducibility, calibration under different temperature. The polymer was characterized with different instrument and proved to have an aging effect as sensing element. In order to achieve an optimized stability, the polymer was mixed with polystyrene and coated on QTF sensor. Over one year stability could be predicted. Calibration response under different temperature has been defined. After optimization, the detection limit is 1ppm. And with application of spin coating, the sensor fabrication could reach within 10% error.

To validate the device performance, field tests have been conducted in multiple locations (including different weather scenarios) and with different sensing technologies. The device has been proved to be useable in several of real-world applications.

To explore more of the device application, a preliminary clinical study was conducted to correlate the hydrocarbon exposure with individual metabolism variance. No significant impact was observed.

The future work will focus on the size and cost optimization due to the need of daily use. With that, it could even be integrated into a smart phone, which will be device free and much more user friendly.

And also, similar approach could be applied for some common small molecule VOCs such as formaldehyde, which is a common air pollutant for indoor air quality control.

REFERENCES

1. Atkinson, R. and J. Arey, *Atmospheric degradation of volatile organic compounds.* Chemical Reviews, 2003. **103**(12): p. 4605-4638.

2. Zhu, X.D. and Y. Liu, *Characterization and Risk Assessment of Exposure to Volatile Organic Compounds in Apartment Buildings in Harbin, China.* Bulletin of Environmental Contamination and Toxicology, 2014. **92**(1): p. 96-102.

3. Goldstein, A.H. and I.E. Galbally, *Known and Unexplored Organic Constituents in the Earth's Atmosphere.* Environmental Science & Technology, 2007. **41**(5): p. 1514-1521.

4. Han, X. and L.P. Naeher, *A review of traffic-related air pollution exposure assessment studies in the developing world.* Environment international, 2006. **32**(1): p. 106-120.

5. *www.epa.gov*.

6. Raaschou-Nielsen, O. and P. Reynolds, *Air pollution and childhood cancer: a review of the epidemiological literature.* International journal of cancer, 2006. **118**(12): p. 2920-2929.

7. Fondelli, M.C., et al., *Benzene exposure in a sample of population residing in a district of Florence, Italy.* Science of the total environment, 2008. **392**(1): p. 41-49.

8. Infante-Rivard, C., *Chemical risk factors and childhood leukaemia: a review of recent studies†.* Radiation protection dosimetry, 2008.

9. Zhao, D., *A Novel Handheld Real-time Carbon Dioxide Analyzer for Health and Environmental Applications*. 2014, Arizona State University.

10. Warneke, C., et al., *Validation of Atmospheric VOC Measurements by Proton-Transfer- Reaction Mass Spectrometry Using a Gas-Chromatographic Preseparation Method.* Environmental Science & Technology, 2003. **37**(11): p. 2494-2501.

11. Rastrello, F., et al., *Thermal Conductivity Detector for Gas Chromatography: Very Wide Gain Range Acquisition System and Experimental Measurements.* Instrumentation and Measurement, IEEE Transactions on, 2013. **62**(5): p. 974-981.

12. Cagan, A., et al., *Fast gas chromatography-differential mobility spectrometry of explosives from TATP to Tetryl without gas atmosphere modifiers.* International Journal for Ion Mobility Spectrometry, 2010. **13**(3-4): p. 157-165.

13. Deng, C., et al., *A Novel Miniaturized Flame Ionization Detector for Portable Gas Chromatography*. Journal of Chromatographic Science, 2005. **43**(7): p. 355-357.

14. Suresh, M., et al., *UV photo-ionization based asymmetric field differential ion mobility sensor for trace gas detection.* Sensors and Actuators B: Chemical, 2014. **195**: p. 44-51.

15. Li, B., et al., *Photo-ionization detectors and associated methods thereof*. 2014, Google Patents.

16. Nyquist, J.E., et al., *Decreased sensitivity of photoionization detector total organic vapor detectors in the presence of methane.* The American Industrial Hygiene Association Journal, 1990. **51**(6): p. 326-330.

17. Smith, P.A., et al., *Hand-held photoionization instruments for quantitative detection of sarin vapor and for rapid qualitative screening of contaminated objects.* Journal of Occupational & Environmental Hygiene, 2007. **4**(10): p. 729-738.

18. *https://monitoringlives.org/category/environmetal-monitoring/*.

19. Fine, G.F., et al., *Metal oxide semi-conductor gas sensors in environmental monitoring.* Sensors, 2010. **10**(6): p. 5469-5502.

20. Barsan, N., M. Schweizer-Berberich, and W. Göpel, *Fundamental and practical aspects in the design of nanoscaled SnO2 gas sensors: a status report.* Fresenius' journal of analytical chemistry, 1999. **365**(4): p. 287-304.

21. Barsan, N. and U. Weimar, *Understanding the fundamental principles of metal oxide based gas sensors; the example of CO sensing with SnO2 sensors in the presence of humidity.* Journal of Physics: Condensed Matter, 2003. **15**(20): p. R813.

22. Vaishanv, V., P. Patel, and N. Patel, *Indium tin oxide thin-film sensor for detection of volatile organic compounds (VOCs).* Materials and manufacturing processes, 2006. **21**(3): p. 257-261.

23. *http://www.versaperm.com/semiconductor_gas_sensors.php*.

24. Gottlich, H., et al., *Noncontact scanning force microscopy based on a modified tuning fork sensor.* Review of Scientific Instruments, 2000. **71**(8): p. 3104-3107.

25. Chen, C., *Portable Wireless Sensors for Personal Exposure and Environmental Monitoring*. 2014, ARIZONA STATE UNIVERSITY.

26. Su, X., et al., *Quartz tuning fork biosensor.* Biosens Bioelectron, 2002. **17**(1-2): p. 111-7.

27. Pelletier, C., et al., *Associations between weight loss-induced changes in plasma organochlorine concentrations, serum T3 concentration, and resting metabolic rate.* Toxicological Sciences, 2002. **67**(1): p. 46-51.

28. Sofuoglu, S.C., et al., *An assessment of indoor air concentrations and health risks of volatile organic compounds in three primary schools.* Int J Hyg Environ Health, 2011. **214**(1): p. 36-46.

29. Rastrello, F., et al., *Thermal Conductivity Detector for Gas Chromatography: Very Wide Gain Range Acquisition System and Experimental Measurements.* Ieee Transactions on Instrumentation and Measurement, 2013. **62**(5): p. 974-981.

30. A. Cagan, H.S., J.E. Rodriguez, G.A. Eiceman, *Fast gas chromatography-differential mobility spectrometry of explosives from TATP to Tetryl without gas atmosphere modifiers.* Int J Ion Mobil Spec, 2010. **13**(9).

31. Chen, C., et al., *A New Sensor for the Assessment of Personal Exposure to Volatile Organic Compounds.* Atmos Environ (1994), 2012. **54**: p. 679-687.

32. Negi, I., et al., *Novel monitor paradigm for real-time exposure assessment.* J Expo Sci Environ Epidemiol, 2011. **21**(4): p. 419-26.

33. Tsow, F., et al., *A Wearable and Wireless Sensor System for Real-Time Monitoring of Toxic Environmental Volatile Organic Compounds.* Ieee Sensors Journal, 2009. **9**(12): p. 1734-1740.

34. Tokonami, S., H. Shiigi, and T. Nagaoka, *Review: micro- and nanosized molecularly imprinted polymers for high-throughput analytical applications.* Anal Chim Acta, 2009. **641**(1-2): p. 7-13.

35. Svenson, J. and I.A. Nicholls, *On the thermal and chemical stability of molecularly imprinted polymers.* Analytica Chimica Acta, 2001. **435**(1): p. 19-24.

36. Corre, Y., M. Seredych, and T.J. Bandosz, *Analysis of the chemical and physical factors affecting reactive adsorption of ammonia on graphene/nanoporous carbon composites.* Carbon, 2013. **55**: p. 176-184.

37. Lunde, P.J. and F.L. Kester, *Chemical and Physical Gas Adsorption in Finite Multimolecular Layers.* Chemical Engineering Science, 1975. **30**(12): p. 1497-1505.

38. Munakata, K., *Reactive vacancy solution theory for correlation and prediction of adsorption equilibria for physical and chemical adsorptions.* Surface Science, 2013. **616**: p. 11.

39. Bloshenko, A.V., et al., *An analysis of absorption-desorption of volatile organic compounds by molecularly imprinted polymer films.* Russian Journal of Physical Chemistry B, 2011. **5**(2): p. 332-344.

40. Gelb, L.D. and K.E. Gubbins, *Characterization of porous glasses: Simulation models, adsorption isotherms, and the Brunauer-Emmett-Teller analysis method.* Langmuir, 1998. **14**(8): p. 2097-2111.

41. Herdes, C. and L. Sarkisov, *Computer simulation of volatile organic compound adsorption in atomistic models of molecularly imprinted polymers.* Langmuir, 2009. **25**(9): p. 5352-9.

42. Wang, R., et al., *Real-time ozone detection based on a microfabricated quartz crystal tuning fork sensor.* Sensors (Basel), 2009. **9**(7): p. 5655-63.

43. M. Avila, M.Z., A. Escarpa, A. Rios, *Molecularly imprinted polymers for selective piezoelectric sensing of small molecules.* Trends in Analytical Chemistry, 2008. **27**.

44. M. Matsuguchi, T.U., *Molecular imprinting strategy for solvent molecules and its application for QCM-based VOC vapor sensing.* Sensors and Actuators B, 2006. **113**: p. 94-99.

45. N. Tsuru, M.K., H. Kawaguchi, S. Shiratori, *A quartz crystal microbalance sensor coated with MIP for "Bisphenol A" and its properties.* Thin Solid Films, 2006. **499**: p. 380-385.

46. K. Yoshizako, K.H., Y. Iwakoshi, K. Kimata and N. Tanaka, *Porogen imprinting effects.* Analytical Chemistry, 1998. **70**: p. 386-389.

47. James A. Goodrich, J.K.K., *Binding and Kinetics for Molecular biologists*. 2006: CSHL Press.

48. Sillman, S., *The relation between ozone, NOx and hydrocarbons in urban and polluted rural environments.* Atmospheric Environment, 1999. **33**(12): p. 1821-1845.

49. Santos, K.A.O., Dantas Neto, A. A.; Moura, M. C. P. A.; Castro Dantas, T. N., *Separation of xylene isomers through adsorption on microporous materials: A review.* Brazilian journal of petroleum and gas, 2011. **5**(4).

50. Yang, Q.H., et al., *Adsorption and capillarity of nitrogen in aggregated multi-walled carbon nanotubes.* Chemical Physics Letters, 2001. **345**(1-2): p. 18-24.

51. Andrievski, R.A., *Review of thermal stability of nanomaterials.* Journal of Materials Science, 2014. **49**(4): p. 1449-1460.

52. Gao, S.Y., Y.P. Koh, and S.L. Simon, *Calorimetric Glass Transition of Single Polystyrene Ultrathin Films.* Macromolecules, 2013. **46**(2): p. 562-570.

53. Williams, M.L., R.F. Landel, and J.D. Ferry, *Mechanical Properties of Substances of High Molecular Weight .19. The Temperature Dependence of Relaxation Mechanisms in Amorphous Polymers and Other Glass-Forming Liquids.* Journal of the American Chemical Society, 1955. **77**(14): p. 3701-3707.

54. Pichon, V. and F. Chapuis-Hugon, *Role of molecularly imprinted polymers for selective determination of environmental pollutants—A review.* Analytica Chimica Acta, 2008. **622**(1–2): p. 48-61.

55. Haupt, K. and K. Mosbach, *Molecularly imprinted polymers and their use in biomimetic sensors.* Chemical Reviews, 2000. **100**(7): p. 2495-2504.

56. He, C., et al., *Application of molecularly imprinted polymers to solid-phase extraction of analytes from real samples.* Journal of biochemical and biophysical methods, 2007. **70**(2): p. 133-150.

57. Tamayo, F., E. Turiel, and A. Mart ń-Esteban, *Molecularly imprinted polymers for solid-phase extraction and solid-phase microextraction: recent developments and future trends.* Journal of Chromatography A, 2007. **1152**(1): p. 32-40.

58. Lavignac, N., C.J. Allender, and K.R. Brain, *Current status of molecularly imprinted polymers as alternatives to antibodies in sorbent assays.* Analytica Chimica Acta, 2004. **510**(2): p. 139-145.

59. Avila, M., et al., *Molecularly imprinted polymers for selective piezoelectric sensing of small molecules.* TrAC Trends in Analytical Chemistry, 2008. **27**(1): p. 54-65.

60. Holthoff, E.L. and F.V. Bright, *Molecularly templated materials in chemical sensing.* Analytica chimica acta, 2007. **594**(2): p. 147-161.

61. Deng, Y., et al., *Aging effect of a molecularly imprinted polymer on a quartz tuning fork sensor for detection of volatile organic compounds.* Sensors and Actuators B: Chemical, 2015. **211**: p. 25-32.

62. Pitten, F.A., J. Bremer, and A. Kramer, *Air contamination with volatile organic compounds (VOC's) and health complaints.* Deutsche Medizinische Wochenschrift, 2000. **125**(18): p. 545-550.

63. Deng, Y., et al. *Unraveling fabrication and calibration of wearable gas monitor for use under free-living conditions*. in *2016 38th Annual International Conference of the IEEE Engineering in Medicine and Biology Society (EMBC)*. 2016.

64. Naghibi, H., A. Tamura, and J.M. Sturtevant, *Significant discrepancies between van't Hoff and calorimetric enthalpies.* Proceedings of the National Academy of Sciences, 1995. **92**(12): p. 5597-5599.

65. Atkins, P. and J. De Paula, *Elements of physical chemistry*. 2013: Oxford University Press, USA.

66. Dickerson, R.E. and I. Geis, *Chemistry, matter, and the universe: an integrated approach to general chemistry*. 1976: Addison Wesley Longman.

67. Arrhenius, S., *Über die Dissociationswärme und den Einfluss der Temperatur auf den Dissociationsgrad der Elektrolyte*. 1889: Wilhelm Engelmann.

68. Brown, K., et al., *Concentrations of Volatile Organic Compounds in Indoor Air – A Review.* Indoor air, 1994. **4**(2): p. 123-134.

69. Win-Shwe, T.-T., et al., *Indoor Volatile Organic Compounds and Chemical Sensitivity Reactions.* Clinical and Developmental Immunology, 2013. **2013**: p. 8.

70. Chagger, H.K., et al., *Emission of volatile organic compounds from coal combustion.* Fuel, 1999. **78**(13): p. 1527-1538.

71. Lerchner, J., D. Caspary, and G. Wolf, *Calorimetric detection of volatile organic compounds.* Sensors and Actuators B: Chemical, 2000. **70**(1–3): p. 57-66.

72. Mart ínez-Hipatl, C., et al., *Detection of volatile organic compounds by an interferometric sensor.* Sensors and Actuators B: Chemical, 2010. **147**(1): p. 37-42.

73. Patel, S.V., et al., *Chemicapacitive microsensors for volatile organic compound detection.* Sensors and Actuators B: Chemical, 2003. **96**(3): p. 541-553.

74. Lingg, R.D., et al., *Quantitative Analysis of Volatile Organic Compounds by GC-MS.* Journal (American Water Works Association), 1977. **69**(11): p. 605-612.

75. Kosterev, A.A., et al., *Applications of quartz tuning forks in spectroscopic gas sensing*. Review of Scientific Instruments, 2005. **76**(4): p. 043105.

76. Zheng, H., X. Zhao, and J. Di, *Hydrogen Sulfide Removal From Petroleum Refinery by Immobilized Thiobacillus ferrooxidans in Fixed-bed Bioreactor.* Petroleum Science and Technology, 2009. **27**(18): p. 2134-2144.

77. Klouda, G.A. and M.V. Connolly, *Radiocarbon (14C) measurements to quantify sources of atmospheric carbon monoxide in urban air.* Atmospheric Environment, 1995. **29**(22): p. 3309-3318.

78. Thomson, G.W., *The Antoine Equation for Vapor-pressure Data.* Chemical Reviews, 1946. **38**(1).

79. Weisel, C.P., et al., *Relationships of Indoor, Outdoor, and Personal Air (RIOPA). Part I. Collection methods and descriptive analyses.* Research report (Health Effects Institute), 2005(130 Pt 1): p. 1-107; discussion 109-27.

80. Brown, S.G., A. Frankel, and H.R. Hafner, *Source apportionment of VOCs in the Los Angeles area using positive matrix factorization.* Atmospheric Environment, 2007. **41**(2): p. 227-237.

81. Grober, R.D., et al., *Fundamental limits to force detection using quartz tuning forks.* Review of Scientific Instruments, 2000. **71**(7): p. 2776-2780.

82. Friedt, J.-M. and É. Carry, *Introduction to the quartz tuning fork.* American Journal of Physics, 2007. **75**(5): p. 415-422.

83. society, P.s.a., *A quick derivation relating altitude to air pressure.* 2004.

84. Surridge, A.D., *Extrapolation of the nocturnal temperature inversion from ground-based measurements.* Atmospheric Environment (1967), 1986. **20**(4): p. 803-806.

85. Yaturu, S., *Obesity and type 2 diabetes.* Journal of Diabetes Mellitus, 2011(1): p. 79-95.

86. Friedman, J.M., *Obesity: Causes and control of excess body fat.* Nature, 2009. **459**(7245): p. 340-342.

87. Pi-Sunyer, X., *A Clinical View of the Obesity Problem.* Science, 2003. **299**(5608): p. 859-860.

88. S., R., *Obesity: the disease of the twenty-first century.* International journal of obesity, 2002. **26**: p. S2-S4.

89. Bloomer, R.J., et al., *Effect of oral intake of capsaicinoid beadlets on catecholamine secretion and blood markers of lipolysis in healthy adults: a*

randomized, placebo controlled, double-blind, cross-over study. Lipids in Health and Disease, 2010. **9**(1): p. 72.

90. Xian, X., et al., *Personalized indirect calorimeter for energy expenditure (EE) measurement.* Global Journal of Obesity, Diabetes and Metabolic Syndrome, 2014. **2**(1): p. 004-008.

91. Zhao, D., et al., *A pocket-sized metabolic analyzer for assessment of resting energy expenditure.* Clinical Nutrition, 2014. **33**(2): p. 341-347.

92. Weir, J., *New methods for calculating metabolic rate with special reference to protein metabolism. 1949.* Nutrition (Burbank, Los Angeles County, Calif.), 1989. **6**(3): p. 213-221.

93. Harris, J.A. and F.G. Benedict, *A biometric study of human basal metabolism.* Proceedings of the National Academy of Sciences, 1918. **4**(12): p. 370-373.

94. Mifflin, M.D., et al., *A new predictive equation for resting energy expenditure in healthy individuals.* The American journal of clinical nutrition, 1990. **51**(2): p. 241-247.

95. Ruiz, J.R., et al., *Validity of resting energy expenditure predictive equations before and after an energy-restricted diet intervention in obese women.* PLoS One, 2011. **6**(9): p. e23759.

96. Tremblay, A., et al., *Thermogenesis and weight loss in obese individuals: a primary association with organochlorine pollution.* International journal of obesity, 2004. **28**(7): p. 936-939.

97. Imbeault, P., et al., *Weight loss-induced rise in plasma pollutant is associated with reduced skeletal muscle oxidative capacity.* American Journal of Physiology-Endocrinology and Metabolism, 2002. **282**(3): p. E574-E579.

98. Yoshioka, M., et al., *Combined effects of red pepper and caffeine consumption on 24 h energy balance in subjects given free access to foods.* British Journal of Nutrition, 2001. **85**(2): p. 203-211.

99. Yoshioka, M., et al., *Effects of Red-Pepper Diet on the Energy Metabolism in Men.* Journal of Nutritional Science and Vitaminology, 1995. **41**(6): p. 647-656.

100. Westerterp-Plantenga, M.S., A. Smeets, and M.P.G. Lejeune, *Sensory and gastrointestinal satiety effects of capsaicin on food intake.* Int J Obes Relat Metab Disord, 2004. **29**(6): p. 682-688.

101. Wahlqvist, M.L. and N. Wattanapenpaiboon, *Hot foods—unexpected help with energy balance?* The Lancet, 2001. **358**(9279): p. 348-349.

102. Casella, G. and R.L. Berger, *Statistical inference*. Vol. 2. 2002: Duxbury Pacific Grove, CA.